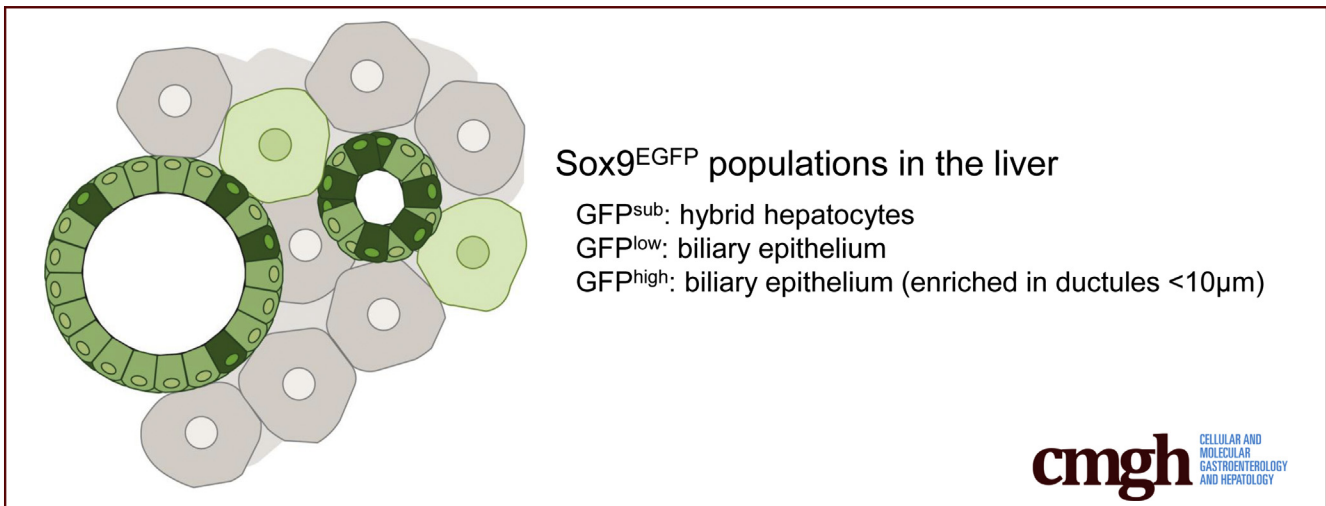


ORIGINAL RESEARCH

Sox9^{EGFP} Defines Biliary Epithelial Heterogeneity Downstream of Yap Activity

Deepthi Y. Tulasi,¹ Diego Martinez Castaneda,¹ Kortney Wager,¹ Connor B. Hogan,⁵ Karel P. Alcedo,² Jesse R. Raab,^{1,3} and Adam D. Gracz^{1,4,5}

¹Department of Genetics, University of North Carolina at Chapel Hill, Chapel Hill, North Carolina; ²Department of Cell Biology and Physiology, University of North Carolina at Chapel Hill, Chapel Hill, North Carolina; ³Lineberger Comprehensive Cancer Center, University of North Carolina at Chapel Hill, Chapel Hill, North Carolina; ⁴Center for Gastrointestinal Biology and Disease, University of North Carolina at Chapel Hill, Chapel Hill, North Carolina; and ⁵Division of Digestive Diseases, Department of Medicine, Emory University, Atlanta, Georgia



SUMMARY

We characterize expression of a Sox9^{EGFP} transgene in the mouse liver. Differential expression of EGFP facilitates identification and isolation of peribiliary hybrid hepatocytes and two biliary epithelial populations with distinct gene expression signatures.

BACKGROUND & AIMS: Defining the genetic heterogeneity of intrahepatic biliary epithelial cells (BECs) is challenging, and tools for identifying BEC subpopulations are limited. Here, we characterize the expression of a Sox9^{EGFP} transgene in the liver and demonstrate that green fluorescent protein (GFP) expression levels are associated with distinct cell types.

METHODS: Sox9^{EGFP} BAC transgenic mice were assayed by immunofluorescence, flow cytometry, and gene expression profiling to characterize in vivo characteristics of GFP populations. Single BECs from distinct GFP populations were isolated by fluorescence-activated cell sorting, and functional analysis was conducted in organoid forming assays. Intrahepatic ductal epithelium was grown as organoids and treated with a Yes-associated protein (Yap) inhibitor or bile acids to

determine upstream regulation of Sox9 in BECs. Sox9^{EGFP} mice were subjected to bile duct ligation, and GFP expression was assessed by immunofluorescence.

RESULTS: BECs express low or high levels of GFP, whereas periportal hepatocytes express sublow GFP. Sox9^{EGFP+} BECs are differentially distributed by duct size and demonstrate distinct gene expression signatures, with enrichment of *Cyr61* and *Hes1* in GFP^{high} BECs. Single Sox9^{EGFP+} cells form organoids that exhibit heterogeneous survival, growth, and HNF4A activation dependent on culture conditions, suggesting that exogenous signaling impacts BEC heterogeneity. Yap is required to maintain Sox9 expression in biliary organoids, but bile acids are insufficient to induce BEC Yap activity or Sox9 in vivo and in vitro. Sox9^{EGFP} remains restricted to BECs and periportal hepatocytes after bile duct ligation.

CONCLUSIONS: Our data demonstrate that Sox9^{EGFP} levels provide readout of Yap activity and delineate BEC heterogeneity, providing a tool for assaying subpopulation-specific cellular function in the liver. (*Cell Mol Gastroenterol Hepatol* 2021;11:1437–1462; <https://doi.org/10.1016/j.jcmgh.2021.01.009>)

Keywords: Biliary Epithelium; Cholangiocytes; Sox9; Yap.

Biliary epithelial cells (BECs) line intrahepatic bile ducts and are responsible for modifying and transporting bile during homeostasis. After acute or chronic liver injury, BECs undergo a proliferative response, termed *ductular reaction*, that is associated with liver repair and modeled in rodents through chemical injury or surgical ligation of the common bile duct. BECs are also impacted by cholangiopathies, which can result in liver failure and have few therapeutic interventions.¹ Evidence suggests a significant degree of functional heterogeneity among BECs with relevance to physiology and liver disease. For example, BEC secretory function is modulated by hormones, peptides, and neurotransmitters, many of which act on a subpopulation of ductal epithelium.¹ BECs also demonstrate differential proliferation after ductal injury, and some BECs are capable of transdifferentiating into hepatocytes after severe or chronic liver injury.^{2–4} However, assigning potentially heterogeneous responses to specific cell “types” is complicated by the fact that BEC subpopulations lack the clear molecular and genetic definitions that have facilitated a deeper understanding of cell biology in other epithelial tissues. New and accessible tools for interrogating BEC heterogeneity are needed to define and dissect context-dependent roles of BEC subpopulations in liver physiology and disease.

BEC heterogeneity has been defined relative to BEC size, with “small” cholangiocytes residing in proximal ductules near the canals of Hering and “large” cholangiocytes in large ducts.⁵ Although isolated bile ducts and immortalized small and large cholangiocyte cell lines have provided significant insight into biliary physiology, size-based definitions complicate isolation of BECs from genetically or pharmacologically challenged livers for direct, *in vivo* insight. Recent single cell transcriptomic studies have shown that BECs demonstrate variable levels of Yes-associated protein (Yap) activity.⁶ Yap activity is increased in bile ducts relative to hepatocytes, and transgenic activation of Yap in hepatocytes drives transdifferentiation to a ductal phenotype.⁷ The Yap pathway and its downstream effectors may present an opportunity for studying BEC heterogeneity from a genetic perspective.

Studies from our lab and others have used a Sox9^{EGFP} BAC transgene to isolate stem, progenitor, and differentiated epithelial cells from mouse intestine and colon.^{8–10} Because Sox9^{EGFP} is expressed broadly and at distinct levels in these tissues, isolation of cells based on green fluorescent protein (GFP) expression provides a single transgene approach to studying cellular heterogeneity. In the liver, Sox9 is a BEC biomarker that is activated during hepatoblast specification into BEC precursors, where it is required for proper timing of biliary differentiation during development.¹¹ We hypothesized that Sox9^{EGFP} could facilitate isolation of BEC subpopulations, similar to previous work in the luminal gastrointestinal tract. Here, we examine Sox9^{EGFP} transgene expression in intrahepatic bile ducts and exploit differential GFP expression levels to isolate distinct cellular subpopulations. Our results demonstrate that Sox9^{EGFP} expression levels facilitate dissection of BEC heterogeneity.

Results

Sox9^{EGFP} Is Expressed in Intrahepatic BECs and Periportal Hepatocytes

We sought to determine whether the Sox9^{EGFP} BAC transgene, previously established as a stem/progenitor cell marker in intestinal and colonic epithelium, accurately labels known Sox9⁺ populations in the liver. Low magnification, epifluorescent imaging of whole liver lobes demonstrated robust GFP signal in branching patterns consistent with intrahepatic bile ducts (Figure 1A). Examination of histologic sections revealed GFP⁺ cells with typical ductal morphology confined to the portal area and co-localized with endogenous SOX9 (Figure 1B). We also observed Sox9^{EGFP} expression throughout the biliary tree, including the gallbladder, extrahepatic bile duct, and pancreatic duct, consistent with known expression patterns of Sox9 in these tissues (Figure 1C–G). In addition, we noted expression of GFP throughout the epithelium of periportal glands in the extrahepatic bile duct, which have been previously reported to express Sox9 and are implicated in regeneration after injury (Figure 1H).¹² Because of independent developmental origins and significant differences in gene expression of biliary epithelium in extrahepatic tissue, we focused the present study on intrahepatic ducts.^{13,14}

To determine whether Sox9^{EGFP} expression accurately labels all BECs and whether Sox9^{EGFP} is restricted to BECs, we next examined enhanced GFP (EGFP) expression relative to the independent BEC markers EPCAM and cytokeratin 19 (K19) by immunofluorescence. In both cases, we found that 100% of BECs identified by EPCAM or K19 were also positive for GFP in left, median, and right lobes (Figure 2A and B). Previous reports have shown that a subpopulation of periportal hepatocytes co-express BEC markers, including Sox9.¹⁵ To test whether Sox9^{EGFP} is also expressed in hybrid hepatocytes, we co-localized GFP⁺ cells with hepatocyte transcription factor HNF4A. We found that a small percentage of Sox9^{EGFP} cells are HNF4A⁺ (Figure 2C). These cells were observed to have typical hepatocyte morphology and express very low levels of the GFP transgene (Figure 2C, *white arrowheads*), in contrast to GFP⁺ cells with BEC morphology, which were appreciably brighter (Figure 2C, *yellow arrowheads*). We did not observe any co-localization between Sox9^{EGFP} and vimentin, which is expressed on mesenchymal, endothelial, and stellate cells (Figure 2D).¹⁶

Finally, we co-localized Sox9^{EGFP} with endogenous SOX9. Surprisingly, we found that some cells expressing the GFP

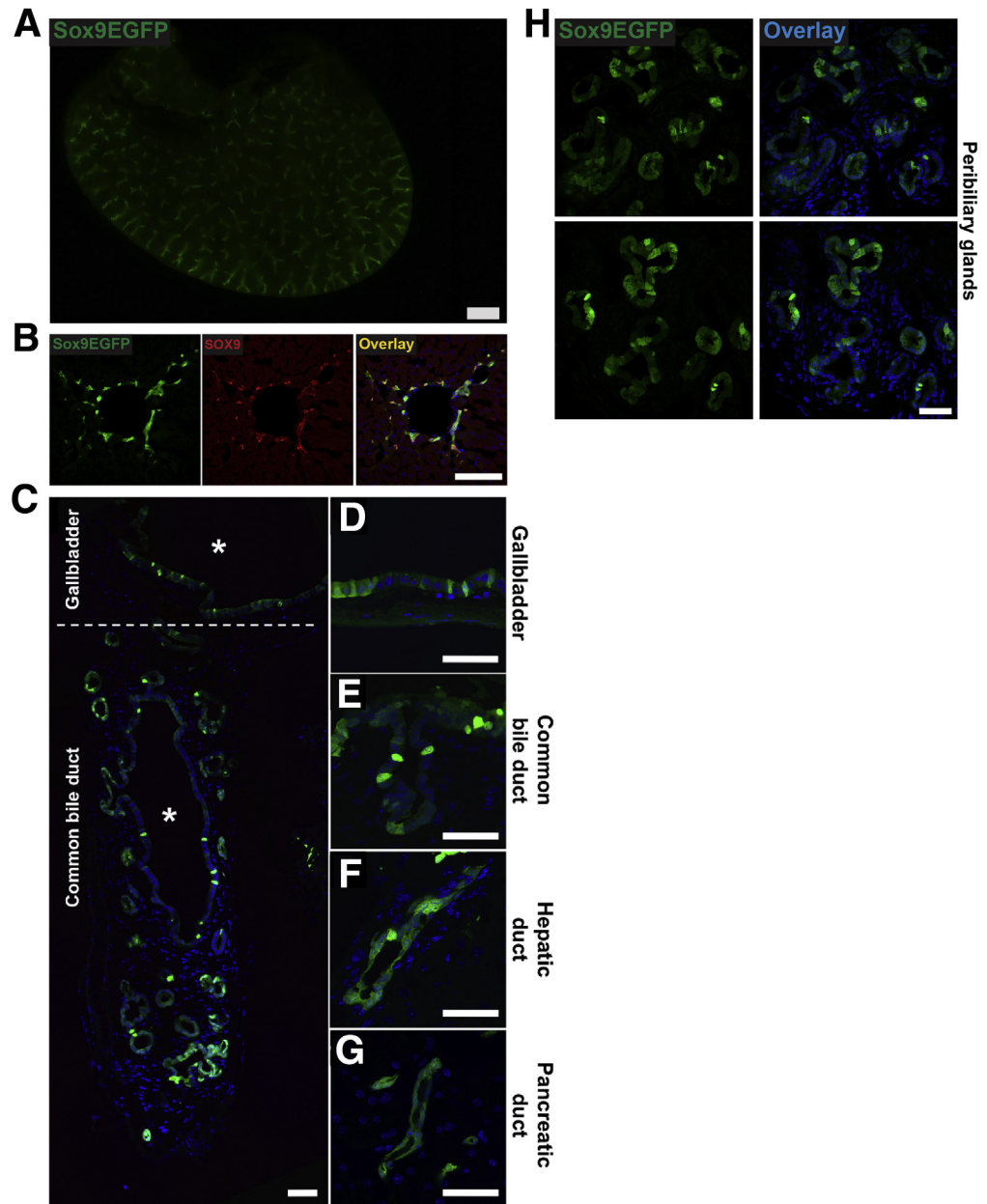
Abbreviations used in this paper: BDL, bile duct ligation; BEC, biliary epithelial cell; DCA, deoxycholic acid; DMEM, Dulbecco modified Eagle medium; EGFP, enhanced green fluorescent protein; FACS, fluorescence-activated cell sorting; FITC, fluorescein isothiocyanate; GFP, green fluorescent protein; K19, cytokeratin 19; LSEC, liver sinusoidal endothelial cell; PBS, phosphate-buffered saline; RT-qPCR, reverse transcriptase quantitative polymerase chain reaction; TNF, tumor necrosis factor; WGA, wheat germ agglutinin; Yap, Yes-associated protein.

 Most current article

© 2021 The Authors. Published by Elsevier Inc. on behalf of the AGA Institute. This is an open access article under the CC BY-NC-ND license (<http://creativecommons.org/licenses/by-nc-nd/4.0/>).

2352-345X

<https://doi.org/10.1016/j.jcmgh.2021.01.009>



transgene did not co-express endogenous SOX9 protein (Figure 3A, arrowheads). The number of GFP⁺/SOX9⁻ cells was not significantly variable between biological replicates. Because SOX9 is considered a pan-biliary marker, we independently confirmed the presence of SOX9⁻ BECs by co-localizing SOX9 with EPCAM by immunofluorescence. We found that SOX9 co-localized with EPCAM⁺ BECs (79.0% \pm 10.5%) at approximately the same rate as EGFP⁺ BECs (77.7% \pm 7.1%) (Figure 3B). Collectively, our immunofluorescence analyses confirm that Sox9^{EGFP} is expressed ubiquitously in BECs, including BECs that lack endogenous SOX9 protein. In addition, very low levels of GFP are expressed in a subpopulation of periportal hepatocytes, consistent with known expression of endogenous Sox9 in hybrid hepatocytes.

GFP^{high} Cells Are More Plentiful in Smaller Ducts

Although qualitative observation demonstrated variable Sox9^{EGFP} expression in intrahepatic bile ducts, we sought to quantify ductal GFP at the single cell level and determine whether different levels of expression correlate with anatomic localization. We used semiquantitative confocal microscopy and measured GFP in individual cells by using wheat germ agglutinin (WGA) to delineate cell membranes. To avoid artifacts associated with antibody detection, all experiments measured endogenous GFP. First, we visually categorized BECs as GFP^{low} or GFP^{high} and asked whether qualitatively identified Sox9^{EGFP} populations demonstrated quantitatively discernible differences in GFP intensity (Figure 2A). We found that BECs identified as GFP^{high} had

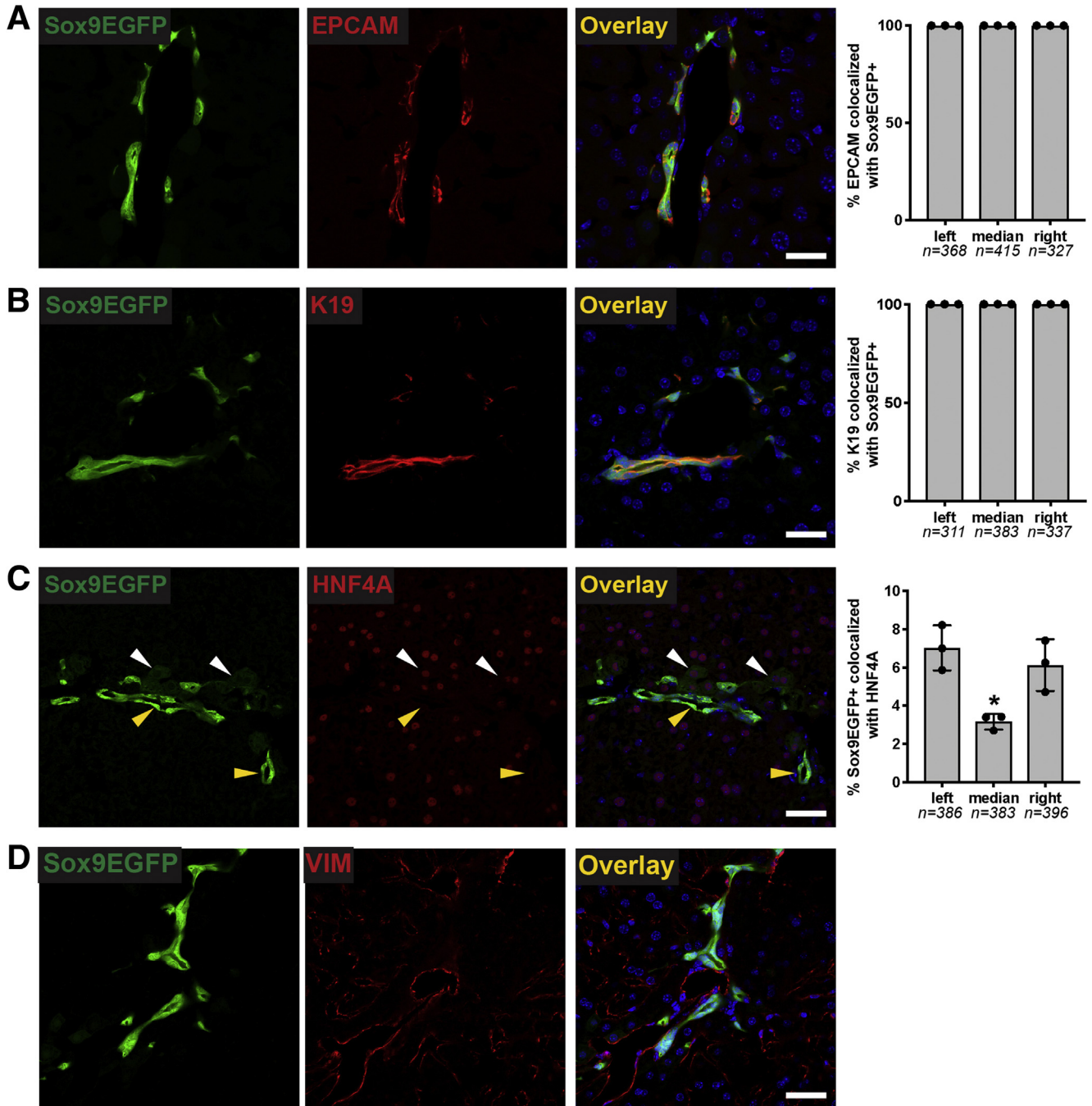


Figure 2. Sox9^{EGFP} is expressed in intrahepatic bile ducts and peribiliary hepatocytes. Immunofluorescence demonstrates that EGFP is co-expressed in (A) 100% of EPCAM⁺ and (B) K19⁺ positive BECs across left, median, and right lobes. (C) Rare peribiliary cells expressing very low levels of EGFP co-localize with HNF4A and are morphologically consistent with hepatocytes (white arrows indicate EGFP⁺/HNF4A⁺; yellow arrows indicate EGFP⁺/HNF4A⁻). (D) Sox9^{EGFP} does not co-localize with mesenchymal marker, vimentin (VIM) (scale bar = 50 μ m).

significantly higher fluorescence intensity relative to those identified as GFP^{low}, validating our ability to resolve Sox9-EGFP populations by histology (Figure 4B).

Because BEC heterogeneity has been classically described relative to cell size and location in small or large ducts, we next quantified GFP expression in individual BECs relative to duct diameter.⁵ GFP fluorescence and duct

diameter of the resident bile duct were measured for 2589 BECs, and we noted a clear inverse relationship between the number of GFP^{high} cells and duct diameter (Figure 4C). To quantify the percentage of GFP^{high} BECs in different-sized ducts, we arbitrarily defined GFP^{high} BECs as having mean fluorescence intensity ≥ 600 , which is based on the upper limit of fluorescence in a majority of GFP^{low} cells

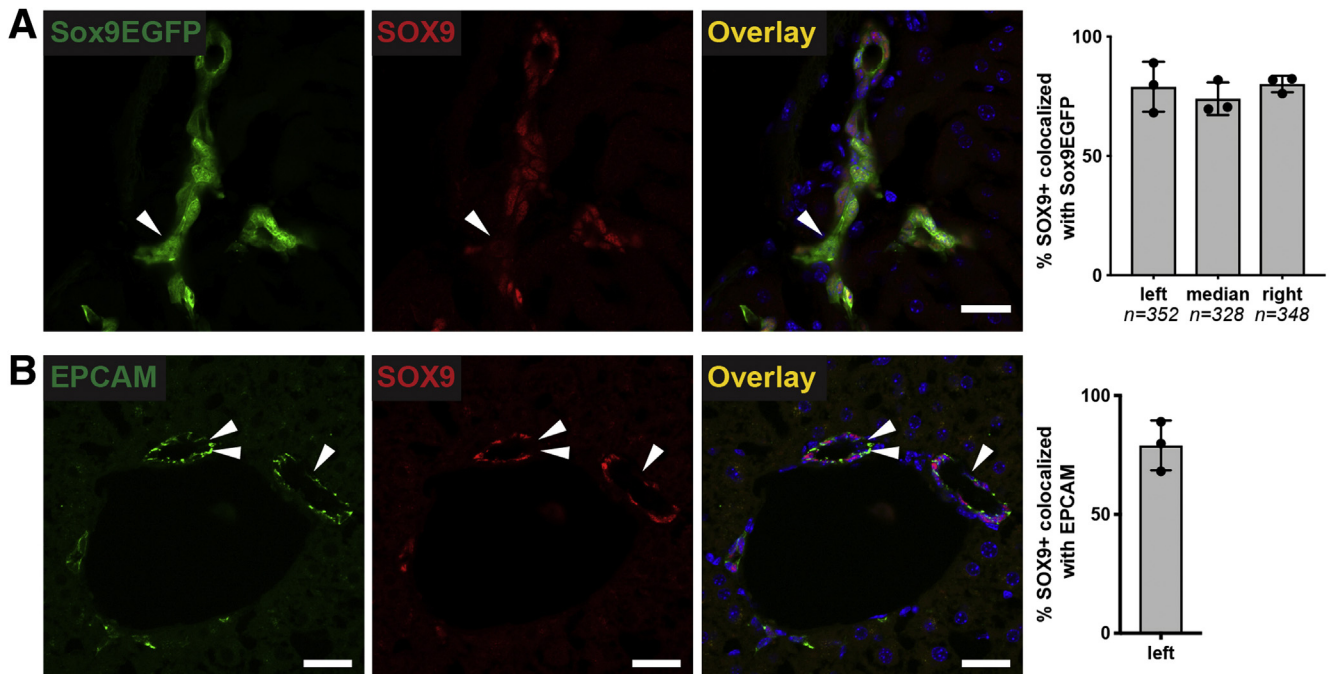


Figure 3. Rare Sox9^{EGFP}-positive BECs do not express SOX9 protein. (A) SOX9 is expressed in most, but not all, Sox9^{EGFP}+ cells (arrowheads indicate EGFP⁺/SOX9⁻) (scale bar = 50 μ m; * indicates $P < .05$, one-way analysis of variance and Tukey test). (B) Co-localization of SOX9 with EPCAM independently confirms the presence and occurrence of SOX9⁻ BECs (left lobe, arrowheads indicate EPCAM⁺/SOX9⁻ cells, scale bars = 50 μ m).

(Figure 4B). Next, we adopted duct size definitions used in recent functional studies of murine intrahepatic biliary epithelium; ducts are defined by a luminal diameter ≥ 10 μ m, and ductules are defined by a luminal diameter of < 10 μ m.² We determined that the smallest ductules (0–5 μ m luminal diameter) are composed of 49.16% GFP^{high} and 50.84% GFP^{low} cells, larger ductules (5–10 μ m luminal diameter) are 18.93% GFP^{high} and 81.07% GFP^{low} cells, and ducts (> 10 μ m luminal diameter) are composed of 4.50% GFP^{high} and 95.50% GFP^{low} cells (Figure 4D). To ask whether cells in the same Sox9^{EGFP} population varied by size relative to their resident duct, we first confirmed that BECs in ducts are larger than BECs in ductules, consistent with previous observations (Figure 4E).¹⁷ Interestingly, cell area was not significantly different between smaller (0–5 μ m) and larger (5–10 μ m) ductules (Figure 4E). Grouping cells by both GFP level and resident duct type revealed that GFP^{high} BECs in ducts are significantly larger than GFP^{high} BECs in ductules, whereas the size of GFP^{low} BECs in ducts and ductules was not significantly different (Figure 4F).

Sox9^{EGFP} is driven by upstream transcriptional regulators of Sox9, and GFP levels accurately predict endogenous SOX9 protein levels in GFP+ cells of the small intestine and colon.^{8,10} We quantified 747 BECs by using WGA and bisbenzimidazole as membrane and nuclear markers for GFP and SOX9 immunofluorescence, respectively (Figure 5A). GFP level was a poor predictor of endogenous SOX9 protein level, and we did not observe specific association of SOX9⁻ cells with low or high GFP expression (Figure 5B). Interestingly, some BECs expressing the highest observed level of

GFP expressed little or no appreciable SOX9. Together, these data demonstrate that Sox9^{EGFP} BECs are compartmentalized by duct size, with GFP^{high} cells present in increased numbers in ductules. Furthermore, GFP^{high} BECs located in ducts are larger than GFP^{high} BECs in ductules. We also find that Sox9^{EGFP} level is not predictive of SOX9 protein expression, in contrast with observations in the small intestine and colon.

Sox9^{EGFP} Expression Levels Facilitate Isolation of Cellular Subpopulations

To further quantify relative levels of Sox9^{EGFP} expression, we analyzed intrahepatic GFP by flow cytometry. Livers were dissociated by using a protocol optimized to obtain single BECs at the expense of hepatocyte viability.¹⁸ Flow cytometry revealed that a majority of cells in our single cell isolations were negative for the GFP transgene (88.7% \pm 6.1%) (Figure 6A and C). Within the GFP+ fraction, we defined 3 distinct subpopulations: GFP^{sublow} (GFP^{sub}), GFP^{low}, and GFP^{high} (Figure 6A and B). Of GFP+ populations, GFP^{high} cells (71.0% \pm 6.1%) were significantly more abundant than GFP^{low} (11.9% \pm 1.8%) and GFP^{sub} (10.6% \pm 4.4%) cells (Figure 6D). These data demonstrate that intrahepatic Sox9^{EGFP} is expressed at distinct levels that can be resolved by flow cytometry.

On the basis of our histologic assays, we reasoned that GFP^{low} and GFP^{high} populations were most likely to represent cells of the intrahepatic bile ducts, whereas GFP^{sub} were likely to represent periportal hepatocytes. To

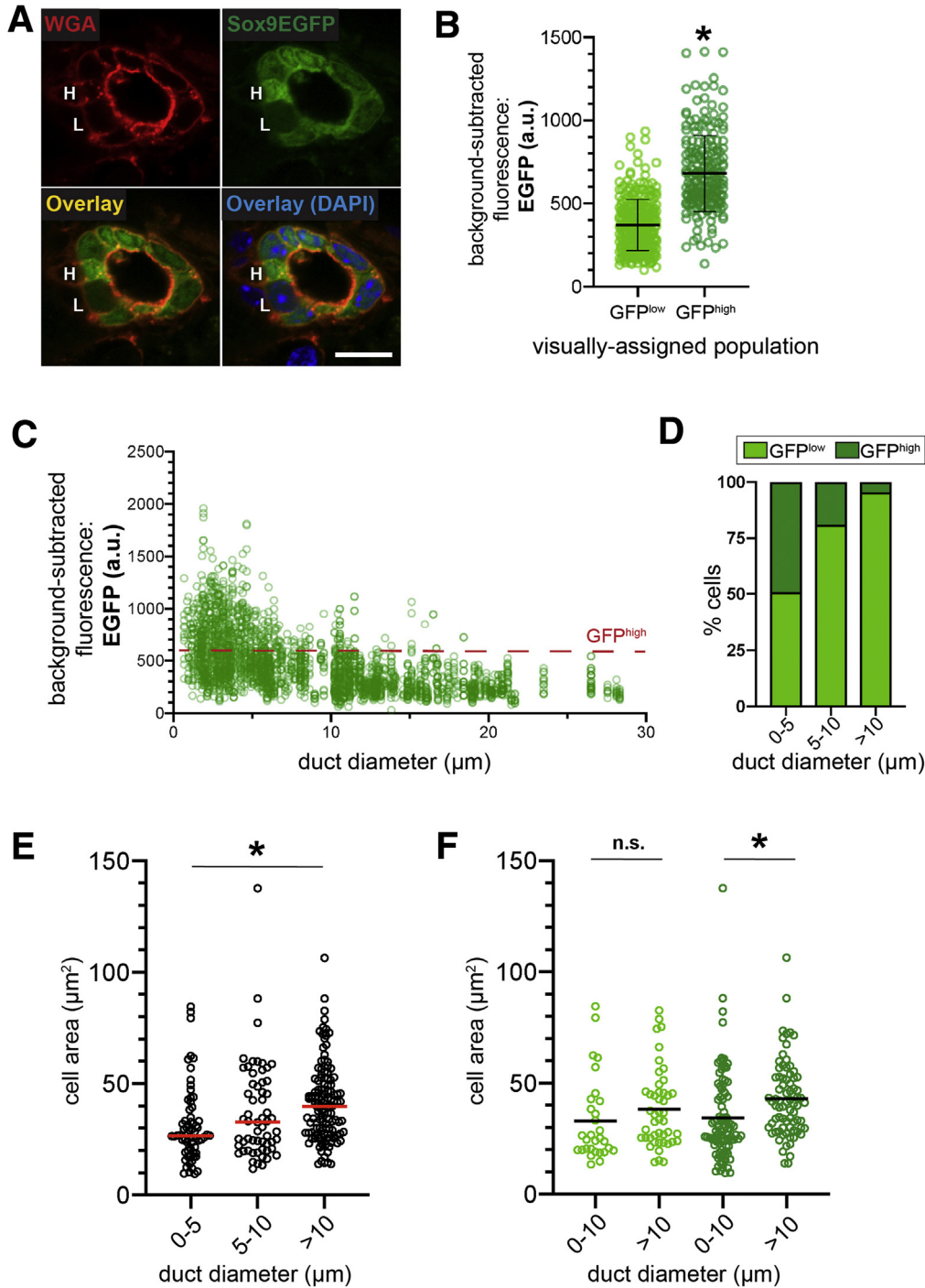


Figure 4. GFP^{high} BECs are enriched in small intrahepatic ductules. (A) WGA labels cell membranes and facilitates quantification of Sox9^{EGFP} cells qualitatively identified as high (H) and low (L) (scale bar = 10 μm). (B) Qualitatively identified GFP^{high} cells are significantly brighter than GFP^{low} cells by quantification of confocal images (n = 307 GFP^{low}, 215 GFP^{high}; * indicates $P < .001$, unpaired t test; a.u. = arbitrary units). (C) Quantification of EGFP intensity relative to duct diameter demonstrates distribution of Sox9^{EGFP} populations across the intrahepatic biliary tree (n = 2589 cells). (D) GFP^{high} BECs are most abundant in small ductules and rare with increasing duct size (n = 954 cells 0–5 μm, 523 cells 5–10 μm, 1112 cells >10 μm). (E) BEC size increases with increasing duct diameter, and BECs located in ducts with luminal diameter ≥ 10 μm are significantly larger than BECs located in the smallest ductules (n = 954 cells 0–5 μm, 523 cells 5–10 μm, 1112 cells >10 μm; * indicates $P < .001$, one-way analysis of variance and Tukey test). (F) GFP^{low} BECs located in ductules and ducts do not differ significantly in size, whereas GFP^{high} BECs located in ducts are significantly larger than GFP^{high} BECs located in ductules (* indicates $P = .01$, one-way analysis of variance and Tukey test).

determine whether the size of sorted GFP^{low} and GFP^{high} BECs was consistent with what we observed in vivo, we measured the area of fluorescence-activated cell sorting (FACS) isolated Sox9^{EGFP} cells from the corresponding gates. We found that, on average, isolated GFP^{high} cells were significantly smaller than GFP^{low} cells (Figure 6E). This could be explained by a greater representation of small, ductule-derived BECs in our liver prep or by changes to cell area after dissociation of epithelial tissues.

Sox9^{EGFP} Populations Exhibit Differential Gene Expression Patterns

We next analyzed gene expression in FACS-isolated Sox9^{EGFP} BEC populations. As expected, *Egfp* was differentially expressed across GFP^{neg}, GFP^{sub}, GFP^{low}, and GFP^{high} populations (Figure 7A). *Sox9* was enriched as expected between (1) GFP^{neg} and GFP^{sub} and (2) GFP^{sub} and GFP^{low/high} (Figure 7B). However, we observed no difference in *Sox9* expression between GFP^{low} and GFP^{high}

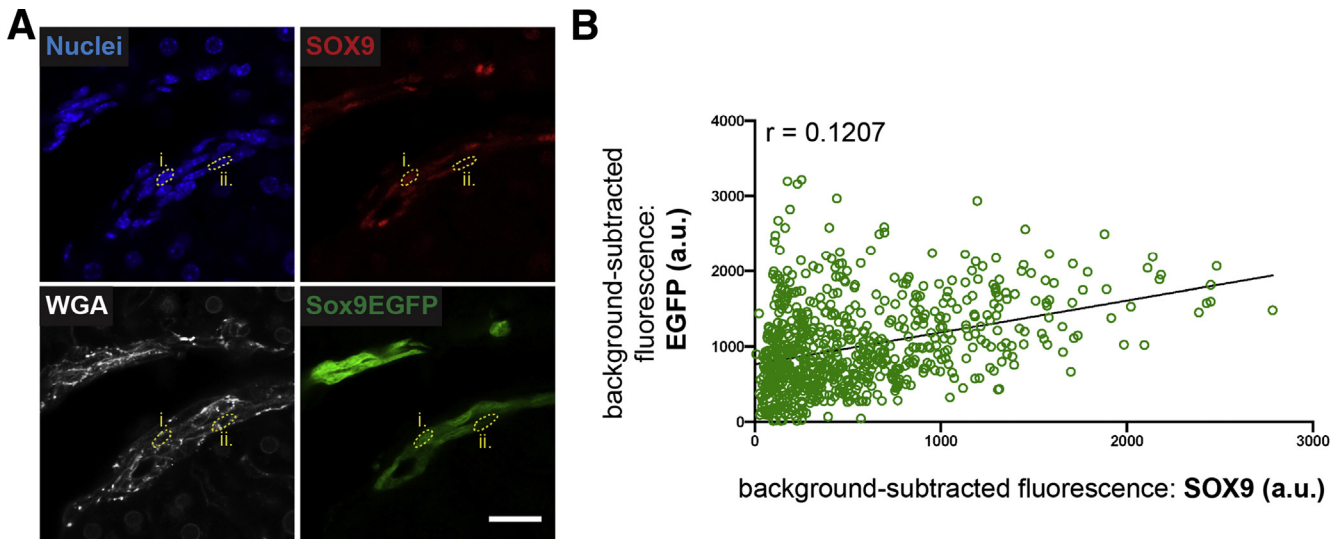


Figure 5. EGFP levels are not predictive of endogenous SOX9 levels. (A) Bisbenzimidazole and WGA label nuclei and cell membranes, respectively, for quantification of SOX9 and EGFP in single cells (*roman numerals* denote cells across multiple channels; scale bar = 25 μ m). (B) SOX9 correlates poorly with EGFP levels ($n = 747$ cells). a.u. = arbitrary units.

populations. We reasoned that differences in post-transcriptional regulation could lead to differential *Egfp* expression without differential *Sox9* expression. To test this hypothesis, we designed reverse transcriptase quantitative polymerase chain reaction (RT-qPCR) primers spanning the second exon and intron of *Sox9* to detect nascent *Sox9* RNA and complement our Taqman assay, which spanned exons 2 and 3 of *Sox9* and is specific to mRNA (Figure 7B). We found that GFP^{high} cells express significantly higher levels of nascent *Sox9* RNA relative to GFP^{low} and GFP^{sub} populations (Figure 7B). These data demonstrate that Sox9^{EGFP} levels provide readout of *Sox9* transcription, which is highest in GFP^{high} BECs despite equivalent amounts of *Sox9* mRNA between GFP^{low} and GFP^{high} populations. This also suggests that *Sox9* undergoes post-transcriptional regulation in BEC subpopulations.

Next, we examined the expression of canonical BEC genes in Sox9^{EGFP} populations. *Spp1*, which encodes pan-biliary marker osteopontin, was significantly enriched in both GFP^{low} and GFP^{high} populations (Figure 7C). Interestingly, although both GFP^{low} and GFP^{high} cells expressed significantly higher levels of *Krt19* relative to GFP^{neg} and GFP^{sub} populations, we observed enrichment of *Krt19* in GFP^{low} relative to GFP^{high} (Figure 7C). To test whether Sox9^{EGFP} populations capture recently reported Yap-associated heterogeneity, we assayed expression of *Cyr61* and *Hes1*, which have been previously correlated with increased Yap activity.^{6,7} Both genes were significantly upregulated in GFP^{high} cells relative to GFP^{low} cells, and *Hes1* was also enriched in GFP^{low} relative to GFP^{sub} (Figure 7D). These data support histologic evidence that GFP^{low} and GFP^{high} cells represent BEC populations, imply distinct transcriptional identities for GFP^{low} and GFP^{high} BECs, and suggest that Sox9^{EGFP} expression levels capture previously described heterogeneity relative to ductal YAP activity.

Unique Transcriptomic Signatures Define Intrahepatic Sox9^{EGFP} Populations

To determine gene expression signatures of Sox9^{EGFP} subpopulations, we conducted RNA-seq on FACS-isolated GFP^{neg}, GFP^{sub}, GFP^{low}, and GFP^{high} populations. Clustering by principal components analysis reinforced expected relationships predicted by histology and RT-qPCR. GFP^{low} and GFP^{high} populations, which are both consistent with BEC identity, clustered together, whereas GFP^{neg} and GFP^{sub} samples demonstrated more significant differences (Figure 8A). Differential gene expression analysis identified genes unique to and shared between Sox9^{EGFP} populations, with the largest shared gene sets consisting of genes shared between GFP^{neg} and GFP^{sub} populations, followed by genes shared between GFP^{low} and GFP^{high} populations (Figure 8B). By comparison, very few genes were shared between GFP^{low/high} and GFP^{sub}, and no genes were shared between GFP^{low/high} and GFP^{neg}.

We next analyzed gene expression signatures of Sox9^{EGFP} populations against published transcriptomic datasets using rank-based gene set scoring.¹⁹ Gene signature analysis demonstrated that GFP^{low} and GFP^{high} were more enriched for intrahepatic BEC-associated genes than GFP^{neg} and GFP^{sub} (Figure 8C).²⁰ All 4 populations were depleted for genes associated with hepatocytes, affirming that our single cell isolation and collection protocol selects against GFP^{neg} hepatocytes. To examine enrichment of known biliary regulatory pathways, we assayed Notch and Yap target genes and again observed significant enrichment in GFP^{low} and GFP^{high} populations (Figure 4C).^{21,22} Although our qPCR data demonstrated differential expression of specific YAP target genes, transcriptome-scale analyses did not reveal a significant difference between GFP^{low} and GFP^{high} populations for either Yap or Notch gene signature scores (Figure 8C). We also examined expression of genes previously associated with functional heterogeneity in small (*Hrh1*) and large (*Cftr*, *Sctr*, *Slc4a2*) cholangiocytes. Surprisingly, both *Hrh1* and *Sctr* were

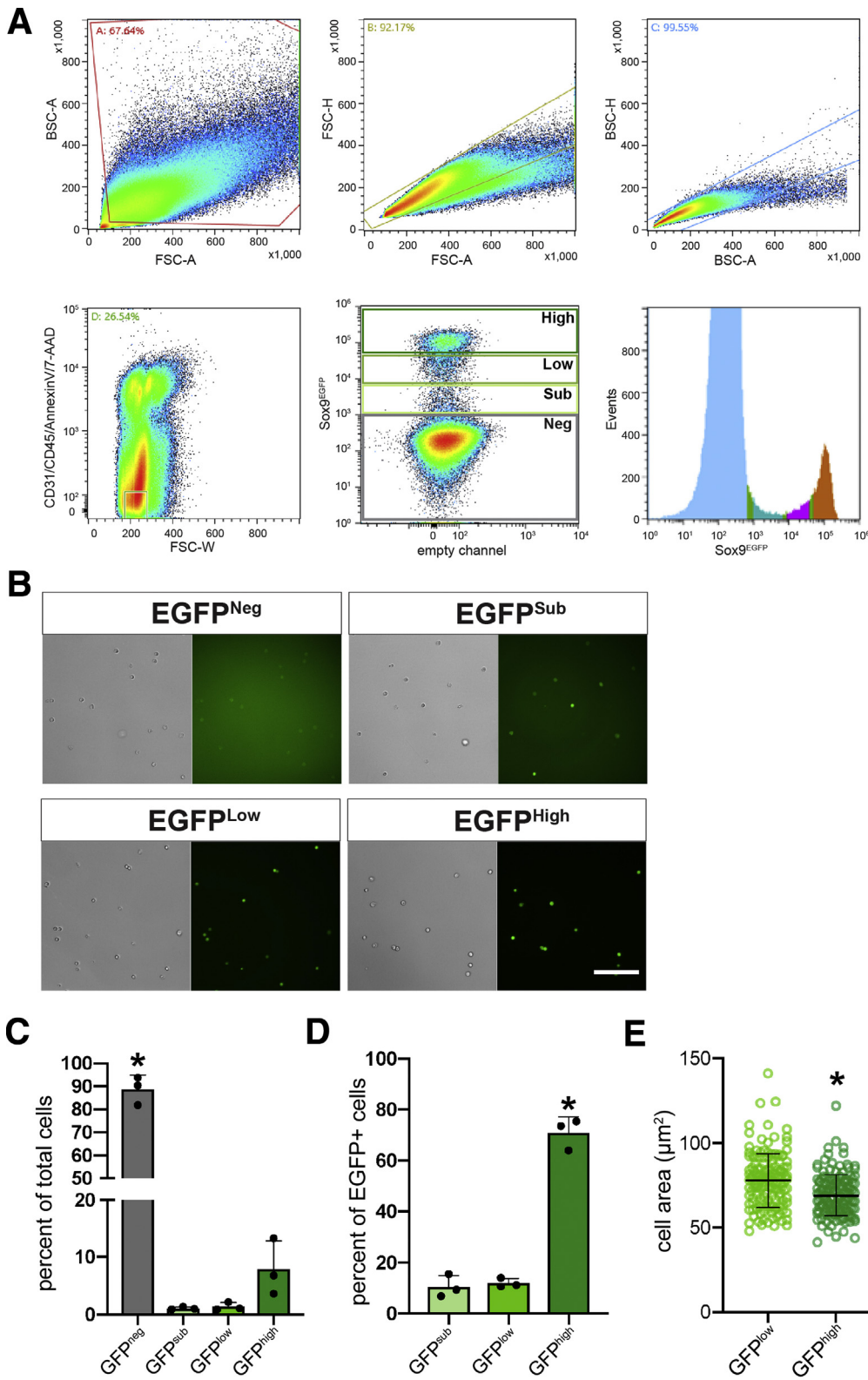


Figure 6. FACS isolation of Sox9^{EGFP} populations. (A) FACS isolation strategy for Sox9^{EGFP} populations demonstrating that Sox9^{EGFP} is divided into 4 populations by flow analysis. (B) FACS-isolated cells from Sox9^{EGFP} populations exhibit increasing EGFP intensity (scale bar = 100 μm). (C) GFP^{neg} cells are the most abundant population present in single cell preps after exclusion of CD31/CD45/Annexin V/7-AAD⁺ cells, and (D) GFP^{high} cells are the most abundant of GFP⁺ populations (* indicates significance, P < .05, one-way analysis of variance and Tukey test). (E) Cell area measurements demonstrate that isolated GFP^{high} cells are significantly smaller than GFP^{low} cells (n = 150 GFP^{low}, 150 GFP^{high}; * indicates P < .001, unpaired t test).

not highly expressed in any Sox9^{EGFP} population from most biological replicates examined (Figure 8D). While *Cftr* and *Slc4a2* were expressed, we did not detect significantly

different levels of expression between GFP^{low} and GFP^{high} BECs, consistent with the localization of both populations in small ductules as well as larger ducts (Figure 8D).

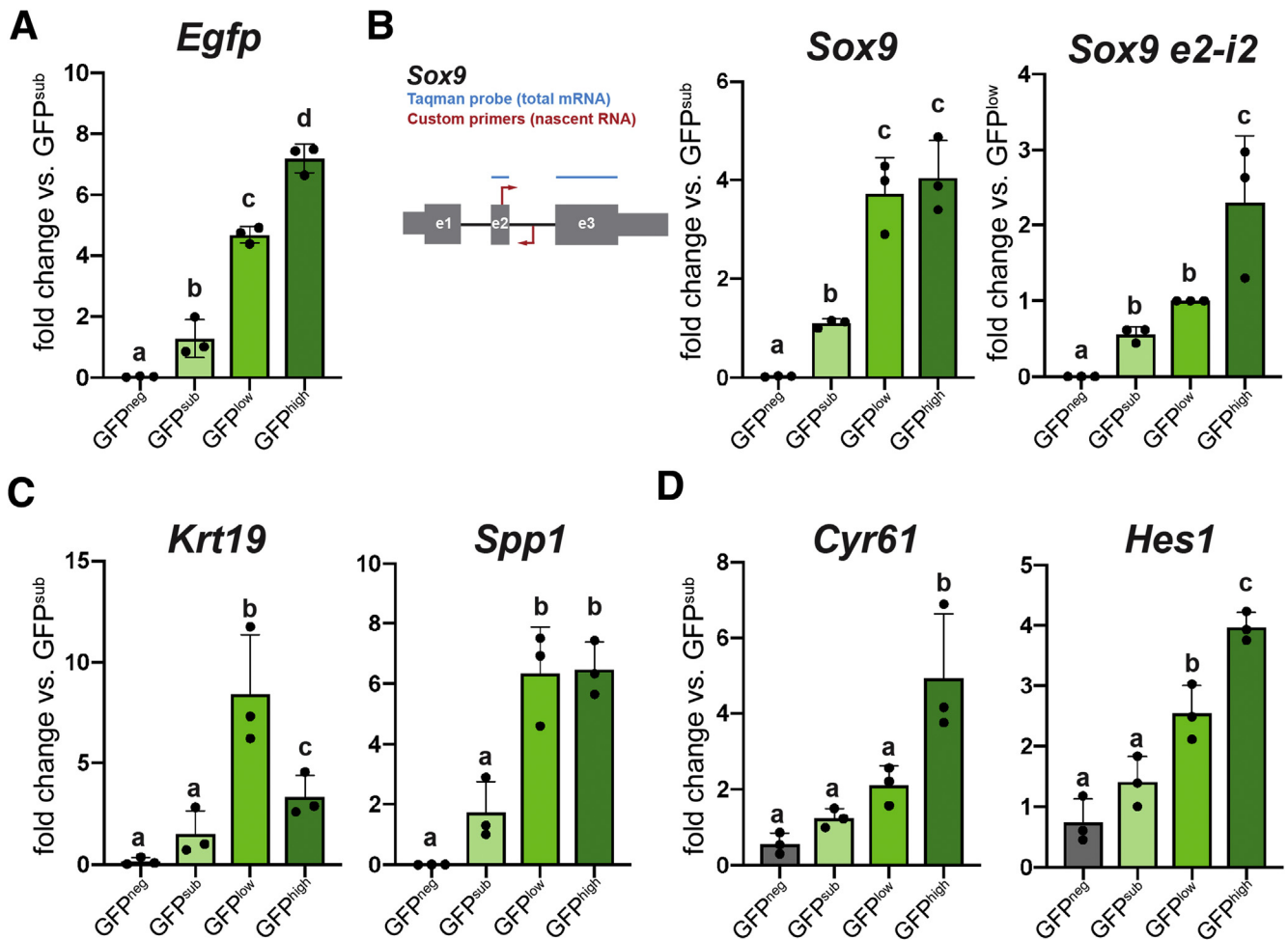


Figure 7. BEC genes demonstrate differential expression across Sox9^{EGFP} populations. (A) *Egfp* expression is significantly different between GFP^{neg}, sub, low, and high populations. (B) RT-qPCR probes detecting *Sox9* mRNA show enrichment between GFP^{neg} and sub populations but not GFP^{low} and high. Primers against nascent *Sox9* RNA demonstrate up-regulation in GFP^{high}. (C) Canonical BEC biomarkers *Krt19* and *Spp1* are differentially expressed in Sox9^{EGFP} populations. (D) *Cyr61* and *Hes1* are most significantly enriched in GFP^{high} cells, suggesting increased Yap activity (letters indicate grouping by significance, $P < .05$, one-way analysis of variance and Tukey test).

To more stringently assay transcriptomic differences between Sox9^{EGFP} populations, we identified genes that were significantly up-regulated in a single population (Figure 8E, Supplementary Tables 1 and 2). Many of the genes uniquely enriched in the GFP^{neg} population were consistent with pericentral liver sinusoidal endothelial cells (LSECs), including *Rspo3*, *Cdh13*, *Flt1*, *Ptgs1*, *Selp*, *Wnt2*, and *Wnt9b* (Figure 8E).²³ Although pericentral LSECs express CD31, it remains restricted to the cytoplasm, explaining why this population would persist in our isolation strategy despite negative selection against CD31 by FACS²⁴ (Figure 6A). The hepatic stellate cell-specific gene, *Lrat*, was also up-regulated in GFP^{neg} cells.²⁵ Although a majority of genes specific to individual GFP⁺ populations have no established function in the liver, we observed gene expression patterns consistent with hybrid hepatocyte and BEC identities. Hepatocyte-associated metabolic enzymes *Cyp1a1* and *Serpina1a* were both up-regulated in GFP^{sub} cells, along with the Hedgehog signaling target *Gli3*. Consistent with our

qPCR data, *Krt19* was significantly enriched in GFP^{low} BECs, along with *Krt17* and WNT pathway genes *Fzd9*, *Wnt7a*, and *Wnt7b*. GFP^{high} BECs expressed *Aqp11*, previously shown to be enriched in developing bile ducts, and *Clu*, which was recently identified as a marker and functional mediator of facultative stem cells in the small intestine (Figure 8E).^{26,27} Together, our transcriptomic data reinforce the broad cellular identities of Sox9^{EGFP} populations defined by histology and RT-qPCR and identify unique gene expression signatures that differentiate GFP^{sub} hybrid hepatocytes and GFP^{low} and GFP^{high} BECs.

Sox9^{EGFP} Populations Exhibit Distinct Phenotypic Responses to Single Cell Organoid Culture

To assay functional properties of proliferation and cell fate in Sox9^{EGFP} populations, we turned to organoid assays. Liver organoids were initially reported to be formed by BECs,

with subsequent studies describing media conditions supportive of hepatocyte organoids.^{28,29} Because the Sox9^{EGFP} transgene is expressed in both a subpopulation of hepatocytes (GFP^{sub}) as well as BECs (GFP^{low} and GFP^{high}), we used conditions developed for BECs (BEC media) as well as conditions developed for hepatocyte organoid culture (tumor necrosis factor [TNF] α media). All GFP⁺ populations formed organoids in both medium conditions, whereas GFP^{neg} cells never formed organoids (Figure 9A). Consistent with previous reports, organoids with clear lumens or spherical morphology took approximately 5–6 days to form, and we quantified organoid formation rates at 7 and 14 days of culture.³⁰ Whereas all GFP⁺ populations formed organoids at approximately the same rate in BEC media, single GFP^{low} and GFP^{high} cells grown in TNF α media formed significantly more organoids than GFP^{sub} cells at both 7 and 14 days of culture (Figure 9B). We observed an increase in GFP^{low}-derived organoids between days 7 and 14, suggesting an extended delay in the ability of some GFP^{low} BECs to form morphologically appreciable organoids in TNF α media (Figure 9B). Furthermore, TNF α media increased organoid formation relative to BEC media in organoids grown from the same GFP⁺ population (Figure 9C).

We quantified organoid area and found that relative to organoids grown in BEC media, organoids grown in TNF α media demonstrated a greater increase in average area between days 7 and 14 in culture, suggesting more robust proliferation induced by TNF α media (Figure 9D). Interestingly, GFP^{sub}- and GFP^{low}-derived organoids were significantly larger than GFP^{high}-derived organoids at day 14 in TNF α media (Figure 9D). Finally, organoids grown in TNF α media were significantly larger than organoids grown in BEC media at both time points and across Sox9^{EGFP} populations (Figure 9E).

To determine whether organoids derived from different Sox9^{EGFP} populations exhibited distinct gene expression profiles, we conducted qPCR on organoids grown in BEC and TNF α media for 7 days. Although we observed some trends in expression for most genes examined, variability between biological replicates resulted in few significant differences between Sox9^{EGFP} populations or medium conditions. Whereas *Sox9* and *Spp1* were not differentially expressed, *Krt19* remained up-regulated in GFP^{low}-derived organoids grown in TNF α media relative to all organoids grown in BEC media and GFP^{high}-derived organoids grown in TNF α media (Figure 10A). *Cyr61* was enriched in GFP^{high}-derived BEC media organoids relative to GFP^{sub}-derived TNF α media but was not significantly different between other populations and conditions (Figure 10B). In addition, *Klf6* trended toward enrichment in GFP^{low}-derived organoids grown in both medium conditions (Figure 10B). Despite increased organoid size and the use of WNT agonist CHIR99021 in TNF α media, Wnt targets *Ccnd1* and *Myc* were not significantly up-regulated in organoids grown in TNF α media, consistent with recent reports of WNT-independence in biliary organoids (Figure 10C).³¹ To determine whether BECs isolated from distinct Sox9^{EGFP} populations produced organoids enriched for small or large cholangiocyte-associated genes, we examined expression of

Cftr, *Hrh1*, *Sctr*, and *Slc4a2*. Of these, only *Slc4a2* was detected by RT-qPCR. *Slc4a2* demonstrated trends in expression between different Sox9^{EGFP} populations and medium conditions, but no significant differences were observed, likely because of variability between biological replicates (Figure 10D). Notably, recent studies of biliary organoid development from single cells also demonstrated repression of some biliary markers at early time points, suggesting that culture conditions may impact expression of some functional cholangiocyte genes.³⁰

Our results demonstrate that organoid-forming capacity is restricted to Sox9^{EGFP} populations but suggest that GFP^{sub}, GFP^{low}, and GFP^{high} cells perform similarly in organoid assays in terms of survival and gene expression. Our data also demonstrate that the most pronounced differences in organoid survival and size were found between medium conditions rather than Sox9^{EGFP} populations. Furthermore, significant interpopulation differences between organoid survival, size, and *Krt19* expression were found exclusively in TNF α media, suggesting that functional heterogeneity of BECs may be driven by exogenous conditions.

Sox9^{EGFP} Populations Demonstrate Different Rates of Transdifferentiation

Previous reports have indicated that BECs are capable of transdifferentiating into hepatocytes, and vice versa, in defined organoid culture systems.^{28,32} Because TNF α media conditions were developed for long-term hepatocyte organoid culture, we reasoned that BEC vs hepatocyte fate decisions might differ between BEC media and TNF α media. To assay cellular identity, we examined protein expression of SOX9 and hepatocyte-specific transcription factor HNF4A by whole-mount immunofluorescence in single cell-derived Sox9^{EGFP} organoids after 7 days of culture in BEC or TNF α media (Figure 11A). Hepatocytes were isolated by collagenase perfusion and grown in TNF α media as positive controls for hepatocyte identity and HNF4A expression (Figure 11C and D). Organoids produced by single GFP^{sub} and GFP^{low} cells expressed SOX9 exclusively in BEC media, whereas a small number of GFP^{high}-derived organoids (8.0%) co-expressed SOX9 and HNF4A (Figure 11B, Table 1). Interestingly, rare GFP^{high}-derived organoids were also observed to be negative for both SOX9 and HNF4A, consistent with SOX9⁻/GFP⁺ BECs observed in vivo.

Single cells grown in TNF α media produced organoids that were more likely to express HNF4A relative to single cells grown in BEC media, regardless of which Sox9^{EGFP} population they were derived from (Figure 5E). Strikingly, although GFP^{sub}-derived organoids did not express HNF4A in BEC media, 100% co-expressed SOX9 and HNF4A in TNF α media. SOX9 and HNF4A were also co-expressed in a larger proportion of GFP^{high}-derived organoids (77.4%) in TNF α media versus GFP^{low} (56.8%) (Figure 11B). Only collagenase-isolated hepatocytes produced organoids expressing HNF4A in the absence of SOX9 (Figure 11B). Next, we examined gene expression of *Hnf4a* and *Cyp51*, which were previously reported to be up-regulated in Lgr5^{EGFP+} liver organoids in

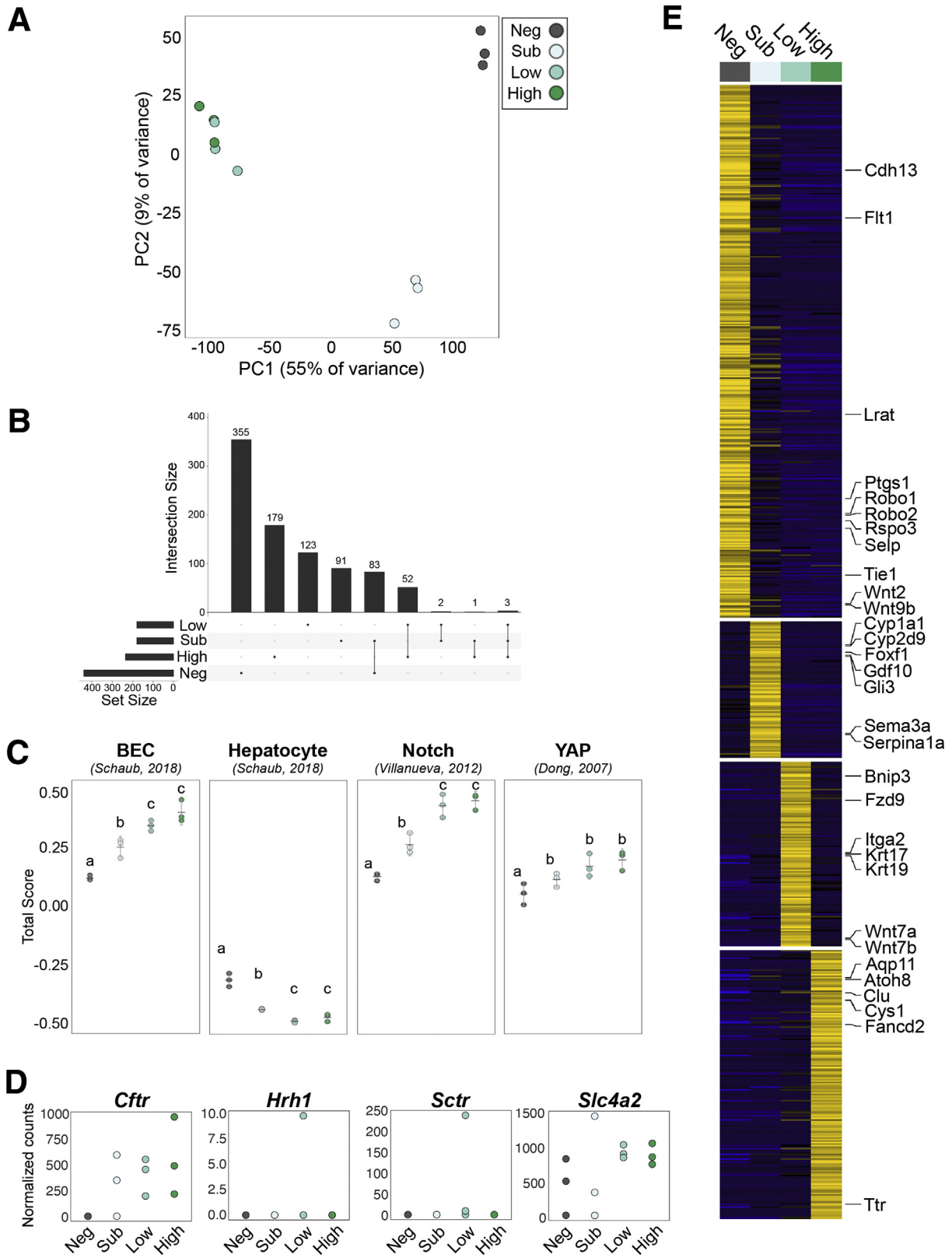


Figure 8. Sox9^{EGFP} populations have distinct transcriptomes. (A) GFP^{neg} and ^{sub} populations form distinct clusters by principal components analysis, whereas GFP^{low} and ^{high} cluster similarly. (B) Genes shared between multiple populations reinforce similarities between GFP^{low} and ^{high}. (C) Gene signature analysis demonstrates significant enrichment of BEC, Notch, and Yap gene sets in GFP^{low} and ^{high} populations relative to GFP^{neg} and ^{sub}, whereas all populations are depleted for hepatocyte genes (error bars represent 95% confidence interval; letters indicate grouping by significance, $P < .05$, one-way analysis of variance and Tukey test). (D) Expression of small and large cholangiocyte markers in Sox9^{EGFP} populations by RNA-seq. (E) Heatmap represents genes uniquely up-regulated in a single Sox9^{EGFP} population.

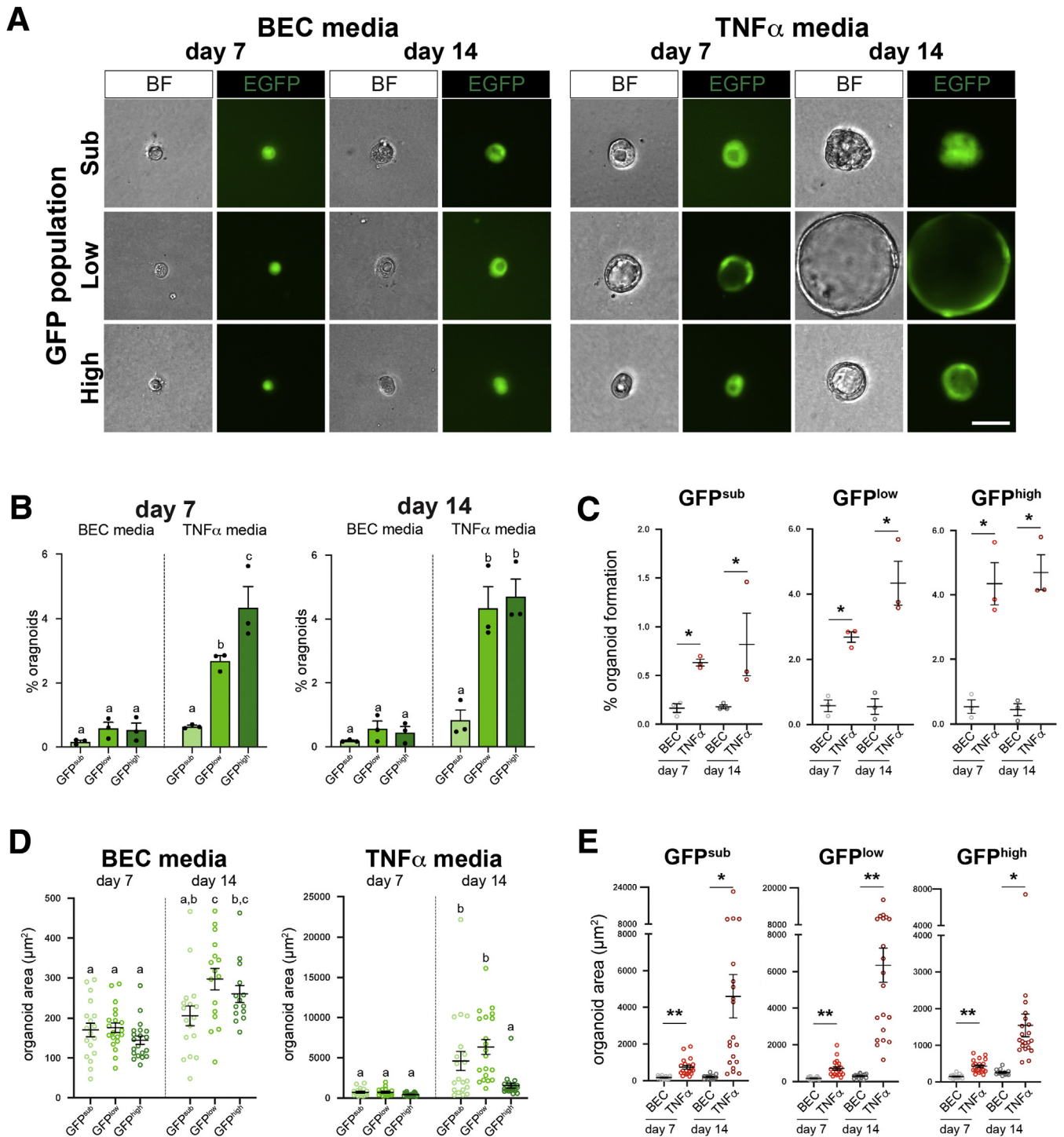


Figure 9. Functional differences in organoids derived from single GFP⁺ cells are dependent on medium conditions. (A) Single cells from Sox9^{EGFP} populations form organoids in medium conditions developed for BECs (BEC media) and hepatocytes (TNF α media) (scale bar = 25 μm). (B and C) TNF α media significantly increase organoid formation relative to BEC media in all Sox9^{EGFP} populations and are required for significantly different organoid formation rates between GFP^{sub}, GFP^{low}, and GFP^{high} (B); letters indicate grouping by significance, $P < .05$, one-way analysis of variance and Tukey test; (C) * indicates significance, $P < .01$, unpaired t test. (D and E) TNF α media also drive more significant increases in organoid size between 7 and 14 days of culture and result in significantly larger GFP^{sub}- and GFP^{low}-derived organoids at day 14 relative to GFP^{high}-derived organoids at the same time point (D); letters indicate grouping by significance, $P < .05$, one-way analysis of variance and Tukey test; (E): * indicates significance, $P < .002$; ** indicates significance, $P \leq .0001$, unpaired t test.

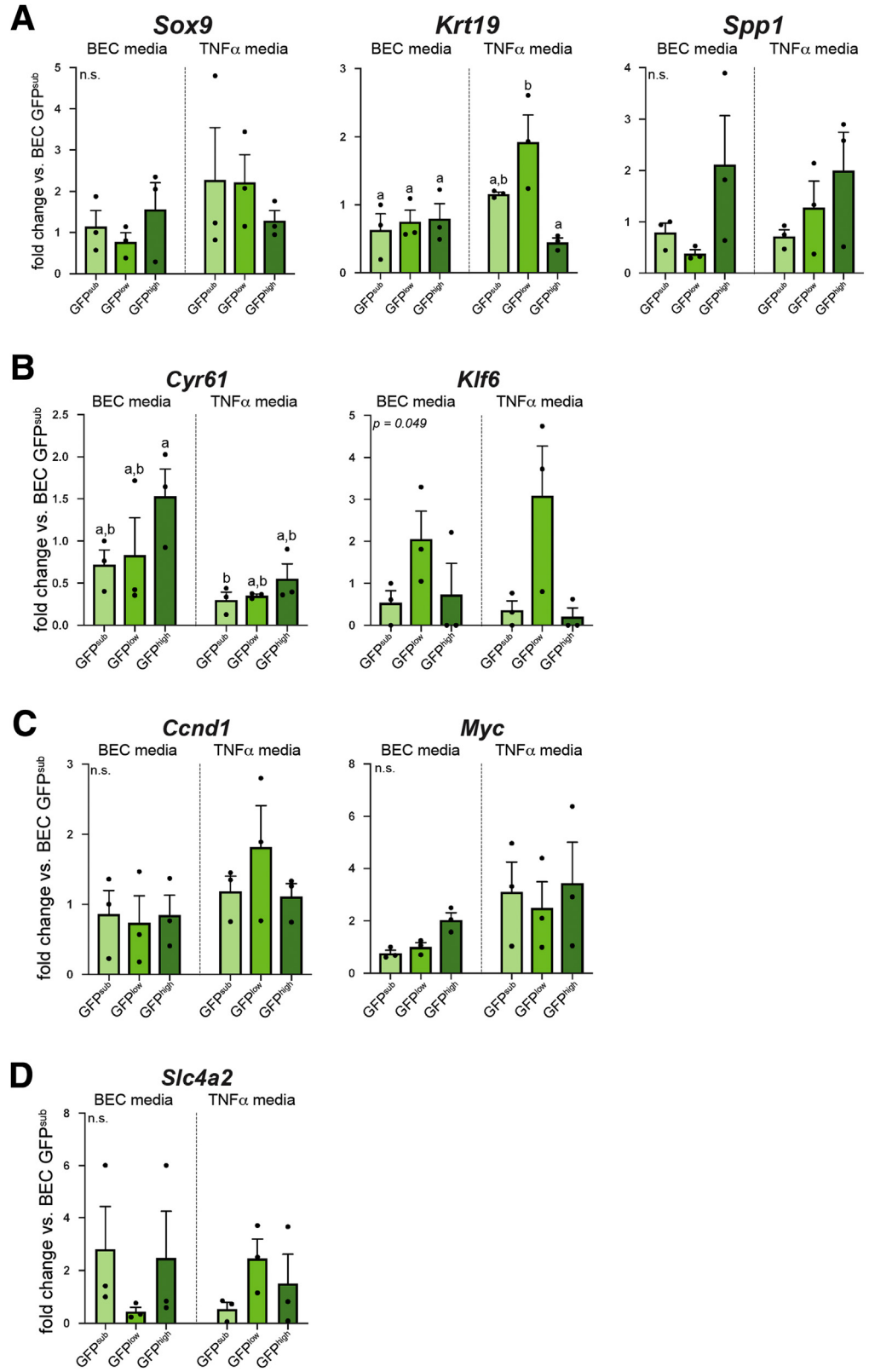


Figure 10. Biliary genes exhibit similar expression across organoids derived from different Sox9^{EGFP} subpopulations. (A) *Sox9* and *Spp1* are not differentially expressed in BEC or TNF α media, but *Krt19* is enriched in GFP^{low}-derived organoids relative to GFP^{high}-derived organoids in TNF α media only, exhibiting an expression pattern similar to in vivo results. (B) *Cyr61* is significantly up-regulated in GFP^{high}-derived BEC media organoids relative to GFP^{sub}-derived TNF α media. Although *Klf6* is not significantly regulated between populations and conditions, it trends toward increased expression in GFP^{low}-derived organoids in both BEC and TNF α media. (C) WNT target genes *Myc* and *Ccnd1* are not differentially expressed between populations and conditions (letters indicate grouping by significance, $P < .05$, one-way analysis of variance and Tukey test; n.s. = not significant).

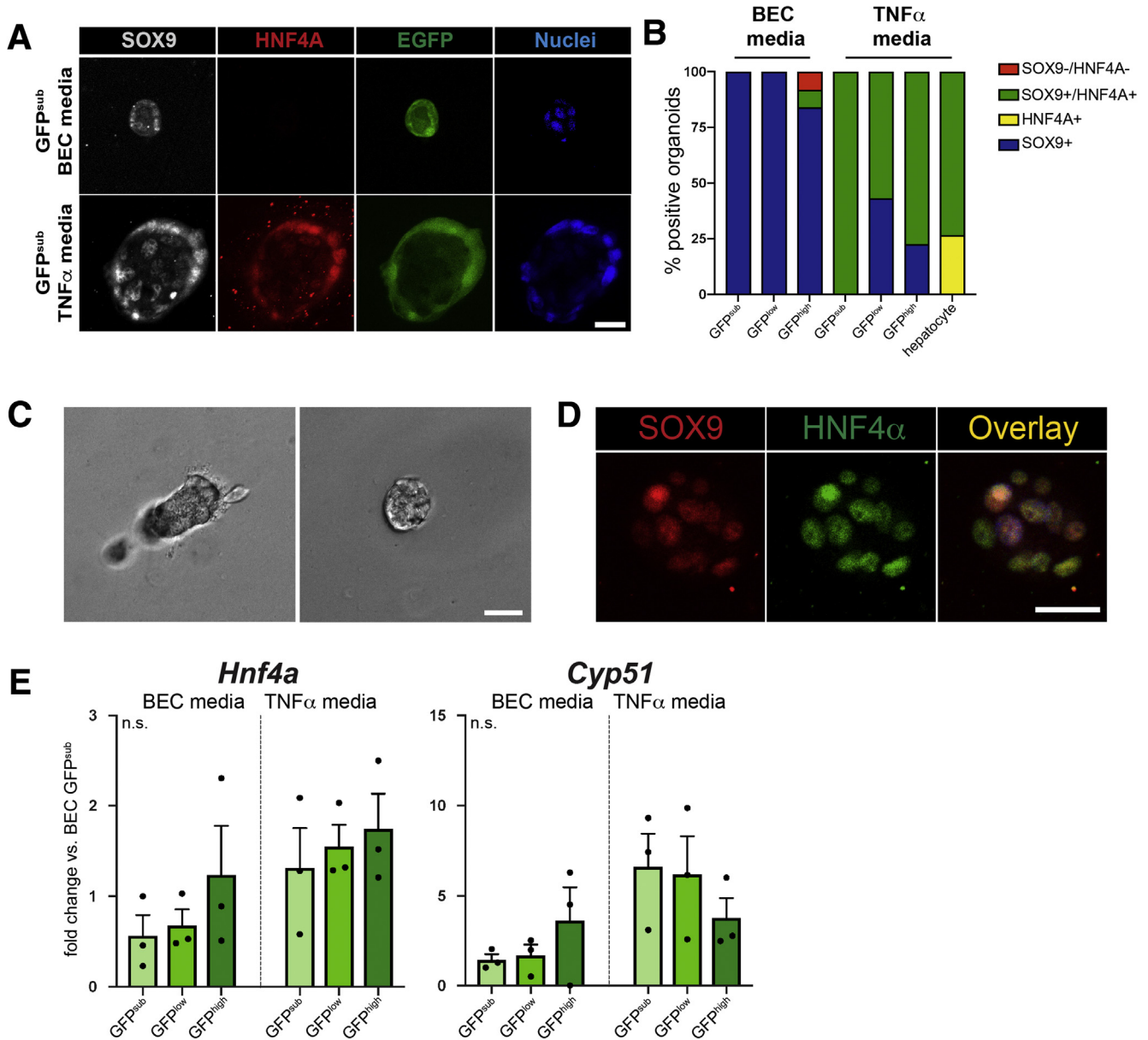


Figure 11. HNF4A expression in single cell derived organoids is dependent on culture conditions and Sox9^{EGFP} population. (A) Representative images of SOX9 and HNF4A immunofluorescence in organoids derived from single Sox9^{EGFP} populations (scale bar = 25 μ m). (B) SOX9 and HNF4A expression is dependent on both medium conditions and Sox9^{EGFP} population, with TNF α media driving increased expression of HNF4A in GFP^{sub}, low, and high-derived organoids, but at distinct rates (n per group in Table 1). (C) Representative images of hepatocyte organoids after 7 days in culture (scale bar = 25 μ m). (D) A majority of hepatocyte organoids express both SOX9 and HNF4A in vitro (scale bar = 25 μ m). (E) *Hnf4a* and *Cyp51* gene expression is not significantly different in organoids derived from different Sox9^{EGFP} populations or between medium conditions ($P > .05$, one-way analysis of variance and Tukey test; n.s. = not significant).

hepatocyte media conditions.²⁸ In contrast to HNF4A protein expression, neither gene was differentially expressed across Sox9^{EGFP} populations or medium conditions (Figure 11E). These data demonstrate that organoids derived from Sox9^{EGFP} populations exhibit varying potential to express HNF4A and that HNF4A expression is enhanced in all Sox9^{EGFP} populations by TNF α media conditions. Our gene expression data suggest that HNF4A activation in TNF α media is regulated at the post-transcriptional level.

Sox9 Expression Is Maintained by Yap but Is not Modulated by Bile Acids

Sox9 is known to be activated downstream of Yap activity in diverse cellular contexts, including developing and regenerating hepatocytes and esophageal cancer cells.^{33,34} Because we observed up-regulation of *Cyr61* and *Hes1* in GFP^{high} cells, we hypothesized that Sox9^{EGFP} may serve as readout for Yap in BECs. To test whether biliary Sox9 expression is Yap-dependent, we treated organoids isolated

Table 1. Organoid Quantification for SOX9/HNF4A Co-localization (Related to Figure 11B)

	Media condition						Hepatocytes
	BEC			TNF			
	Sox9 ^{EGFP} population						
	GFP ^{sub}	GFP ^{low}	GFP ^{high}	GFP ^{sub}	GFP ^{low}	GFP ^{high}	
SOX9-/HNF4A-	0	0	4	0	0	0	0
SOX9+/HNF4A+	0	0	4	27	25	41	27
SOX9+/HNF4A-	5	23	42	0	19	12	0
SOX9-/HNF4A+	0	0	0	0	0	0	8
Total organoids	5	23	50	27	44	53	30

from whole bile ducts with verteporfin, a small molecule inhibitor of Yap.³⁵ Verteporfin treatment did not result in appreciable changes to organoid morphology (Figure 12A). As expected, we observed a significant decrease in the expression of Yap target genes *Cyr61* and *Klf6*, as well as *Sox9* (Figure 12B). *Gadd45b*, another known target of Yap signaling, remained unchanged, suggesting differential regulation of canonical Yap targets in biliary epithelium (Figure 12B).

Recent studies have shown that bile acids induce Yap in both hepatocytes and BECs.^{6,36} To test whether biliary *Sox9* is also induced by bile acids upstream of Yap, we administered deoxycholic acid (DCA) to wild-type mice via a single intraperitoneal injection and analyzed gene expression in FACS-isolated EPCAM⁺ BECs 24 hours later (Figure 13A).³⁷ We found that neither *Sox9* nor Yap targets *Cyr61* or *Klf6* were responsive to DCA in vivo (Figure 13B). To identify a BEC-specific positive control gene and validate DCA treatment, we assayed a panel of putative targets of farnesoid X receptor that were identified by published farnesoid X receptor CHIP-seq and expressed in GFP^{low} or GFP^{high} BECs in our RNA-seq.³⁸ Although most candidate target genes were unresponsive to DCA, we observed significant up-regulation of *Il6* in DCA-treated mice relative to vehicle controls, consistent with previous reports of nuclear factor kappa B induction of *Il6* in BECs after bile acid treatment (Figure 13B and C).³⁹

We reasoned that transcriptional responses to bile acid fluctuations in vivo might be subtle and next assayed BEC-autonomous responses to DCA by treating organoids in vitro. We did not observe a change in expression of *Sox9* or Yap target genes at 24 hours of treatment, despite induction of *Il6* in 2 of 3 replicates (Figure 14A). Because DCA-induced Yap was previously shown to be dependent on apical sodium-dependent bile acid transporter (ASBT), which is found on the apical membrane of BECs, we confirmed that DCA was interacting with apical cell surfaces via 2 independent experiments.⁶ First, we treated biliary organoids with fluorescein isothiocyanate (FITC)-conjugated DCA and measured luminal fluorescence 9 hours after treatment. Organoids treated with FITC-DCA exhibited significantly increased luminal fluorescence relative to controls treated with FITC-dextran, indicating that DCA is capable of crossing the basolateral membrane and entering organoid lumens (Figure 14B). Next, we passaged biliary organoids into monolayers, so apical membranes interact directly with overlaid media. As observed in our in vivo and organoid experiments, DCA failed to induce *Cyr61*, *Klf6*, or *Sox9* in biliary monolayers, but *Il6* was significantly up-regulated (Figure 14C). These data demonstrate that biliary *Sox9* expression is maintained by Yap, but that both Yap activity and *Sox9* are unaffected by DCA.

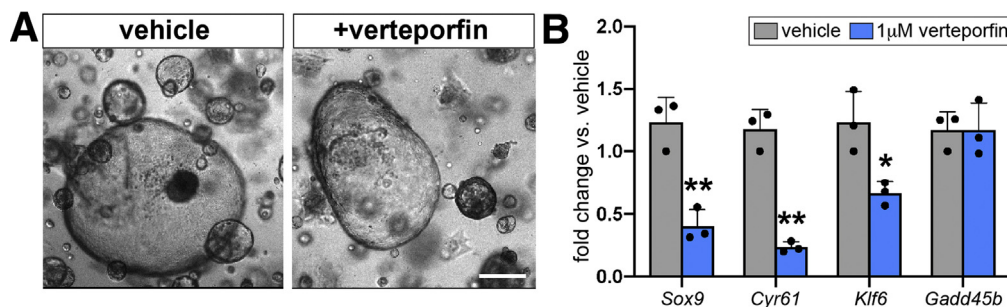


Figure 12. Sox9 expression in BECs is maintained by Yap. (A) Verteporfin treatment does not impact organoid morphology (scale bar = 50 μm) but (B) results in significant down-regulation of *Sox9* and established BEC Yap targets, *Cyr61* and *Klf6*, whereas *Gadd45b* is unaffected (* indicates significance, $P < .05$; ** indicates significance, $P \leq .01$, unpaired t test).

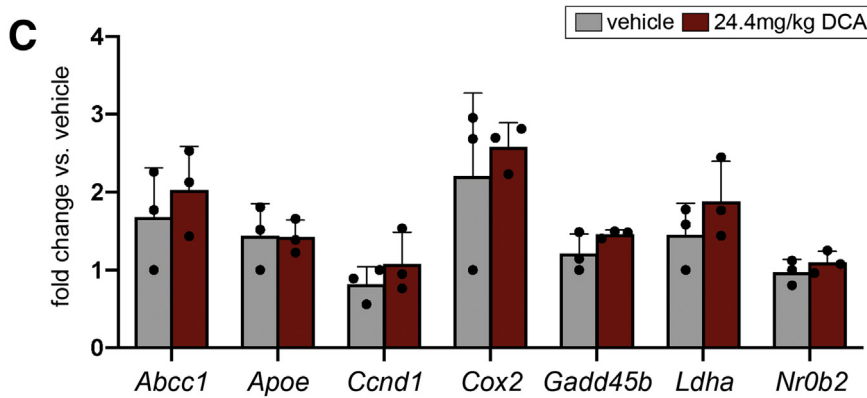
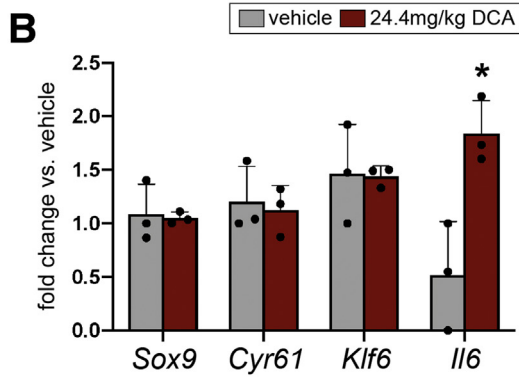
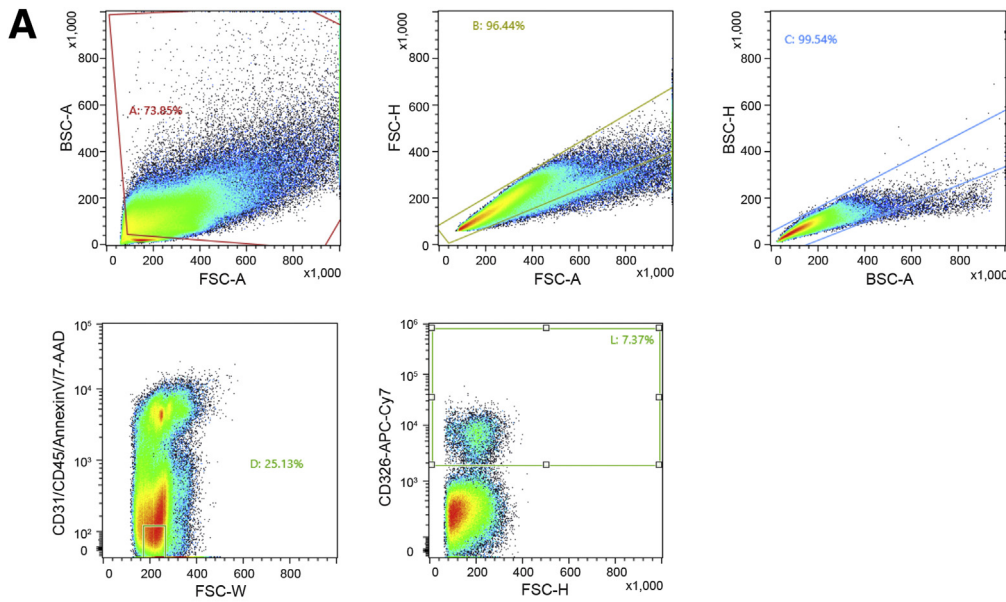


Figure 13. Sox9 expression is not up-regulated by bile acids in vivo. (A) FACS isolation strategy for EPCAM⁺ BECs from vehicle and DCA-treated mice. (B) Sox9 and Yap target genes are not differentially expressed in EPCAM⁺ cells from mice treated with DCA for 24 hours, but Il6 is significantly up-regulated. (C) Candidate DCA targets that were not differentially expressed in isolated BECs after DCA administration in vivo (* indicates significance, $P < .05$, unpaired t test).

Sox9^{EGFP} Is Expressed in BECs and Peribiliary Hepatocytes After Cholestatic Injury

As proof-of-concept for the utility of the Sox9^{EGFP} transgene in studying BECs after liver injury, we examined EGFP expression by histology 7 days after BDL. BDL is a

well-established model of cholestatic injury that is associated with ductular reaction and activation of BEC phenotype in some peribiliary hepatocytes.^{40,41} We observed distinct levels of EGFP expression, along with expansion of EGFP⁺ BECs in portal fields and increase in GFP^{sub} hepatocytes,

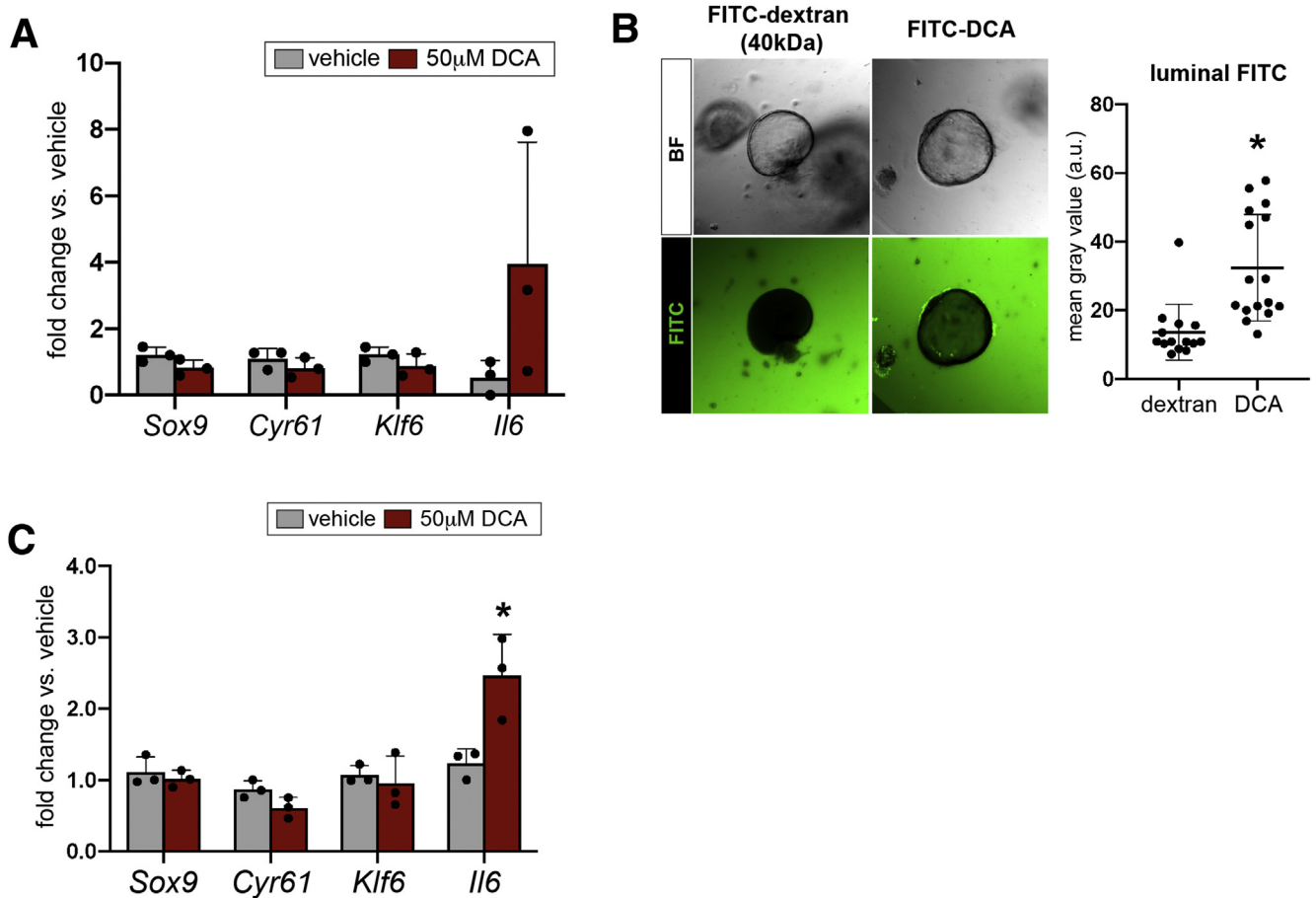


Figure 14. Sox9 expression is not up-regulated by bile acids in vitro. (A) Biliary organoids treated with DCA for 24 hours reproduce in vivo results, failing to up-regulate *Sox9*, *Cyr61*, and *Klf6* and demonstrating heterogeneous response in terms of *Il6* up-regulation. (B) FITC-conjugated DCA was found in organoid lumens after 9 hours of treatment, whereas FITC-dextran was excluded ($n = 16$ FITC-dextran treated organoids, 14 FITC-DCA treated organoids; * indicates significance, $P = .004$, unpaired t test). (C) Primary biliary monolayers treated with DCA in vitro also up-regulated *Il6* but failed to demonstrate significantly different expression of *Sox9*, *Cyr61*, or *Klf6* (* indicates significance, $P < .05$; ** indicates significance, $P \leq .01$, unpaired t test).

consistent with ductular reaction to cholestasis (Figure 15). As in uninjured livers, all EPCAM⁺ and K19⁺ BECs co-expressed the EGFP transgene (Figure 15A and B), whereas a portion of EGFP⁺ cells with hepatocyte morphology and relatively low levels of EGFP co-expressed HNF4A (Figure 15C). Because *Sox9* is known to be expressed in activated stellate cells and is associated with development of fibrosis after injury, we examined expression of alpha-smooth muscle actin and vimentin.^{42,43} We did not observe any co-localization between either marker and the Sox9^{EGFP} transgene (Figure 15D and E, ≥ 10 portal fields from each of 3 mice 7 days after BDL). Finally, we assayed co-localization between EGFP and endogenous SOX9 protein. Although the overall number of SOX9-expressing EGFP⁺ cells was similar to uninjured livers ($77.6\% \pm 13.6\%$ after BDL vs $77.7\% \pm 7.1\%$ uninjured), we noticed that SOX9⁻/EGFP⁺ cells appeared to exclusively demonstrate hepatocyte morphology (Figure 15F, yellow vs white arrowheads). We confirmed that all EPCAM⁺ BECs co-express SOX9 protein, which suggests that the only EGFP⁺

cells that do not express SOX9 after BDL are hepatocytes (Figure 15G). Together, these data demonstrate that Sox9-EGFP expression levels are preserved after cholestatic liver injury induced by BDL, and that the EGFP transgene is expressed in similar cell populations in homeostasis and in the setting of injury/regeneration.

Discussion

Dissecting cellular heterogeneity is important for understanding how subpopulations of cells contribute to tissue homeostasis and disease. Although advances in single cell genomics provide tools for rapid and unbiased cataloguing of cell types, models that facilitate identification and manipulation of cell populations in intact tissues are still critical for understanding cellular function. Here, we characterize Sox9^{EGFP} expression in the liver and establish a tool for understanding heterogeneity in BECs. Sox9^{EGFP} is expressed at variable levels that are associated with phenotypically distinct cell populations in the small

intestine, colon, and pancreatic duct.^{8,10,44} Our data demonstrate variability in Sox9^{EGFP} expression levels throughout the intrahepatic bile ducts and periportal hepatocytes and confirm unique anatomic distribution, gene expression, and functional properties characteristic of each Sox9^{EGFP} population. In the present study, we show that EGFP is not expressed in non-epithelial cells during homeostasis or at 7 days after BDL. However, the known activation of Sox9 in hepatic stellate cells in the setting of chronic fibrosis warrants confirmation of EGFP expression in other injury models.^{42,43} We also observe distinct Sox9^{EGFP} expression levels in the extrahepatic bile ducts and gallbladder, suggesting that the transgene may be a useful biomarker for understanding cellular heterogeneity in these tissues as well. Notably, Sox9^{EGFP} is expressed at variable levels in peribiliary glands, which have been proposed to house BECs with stem cell-like properties.¹² Although the ubiquitous expression of Sox9^{EGFP} and near-ubiquitous expression of endogenous SOX9 in EPCAM⁺ and K19⁺ ductal epithelium suggest that Sox9 itself is unlikely to be a specific biomarker of any one BEC subpopulation, distinct EGFP expression levels may be indicative of cellular heterogeneity throughout the biliary tree.

Unlike previous reports in the intestine, we find that Sox9^{EGFP} does not accurately report endogenous SOX9 protein or mRNA levels. Instead, the highest levels of *Egfp* expression are associated with increased nascent Sox9 RNA. In addition, some GFP⁺ BECs do not express SOX9 protein during homeostasis. Because SOX9 is considered a ubiquitous marker of BECs and is required for BEC specification during development, this observation was unexpected but confirmed by co-localization of EPCAM and SOX9, demonstrating a similar number of SOX9⁺ BECs.¹¹ Interestingly, all BECs express SOX9 after BDL, suggesting that pan-biliary translation of Sox9 mRNA may play an important role in response to injury. The mechanistic significance of the regulation of Sox9 mRNA and protein expression, as well as its impact on adult BEC identity, function, and regeneration, warrants further investigation.

In contrast to other epithelial tissues, the biliary epithelium lacks clearly defined cell populations with compartmentalized functional properties (eg, stem, enteroendocrine, and absorptive cells in intestinal epithelium; type I and type II pneumocytes in alveolar epithelium). This lack of defined populations and general ambiguity of distinctions between cell types in the biliary epithelium complicate defining cell types captured within each Sox9^{EGFP} population, as well as intrapopulation heterogeneity. The clearest distinction found in the present study is between GFP^{sub} hepatocytes and GFP^{low/high} BECs. Sox9 expressing hybrid hepatocytes have been previously defined by their peribiliary anatomic location and co-expression of hepatocyte and BEC markers.¹⁵ GFP^{sub} cells are localized to the peribiliary niche, co-express HNF4A in vivo, and demonstrate enrichment of BEC genes by transcriptomic signature analysis, consistent with hybrid hepatocytes. Interestingly, GFP^{sub}-derived organoids exclusively expressed SOX9 in BEC media and always co-expressed SOX9 and HNF4A in TNF α media. Although the low rate of

organoid formation precluded functional assays in the present study, these data suggest bipotency of GFP^{sub} cells and their progeny. We also observed an increase in GFP^{sub} hepatocytes after BDL, consistent with previous reports of Sox9 activation in peribiliary hepatocytes after injury to the bile ducts.⁴¹ Accordingly, the Sox9^{EGFP} transgene may be a useful tool for differentially assessing BEC and hybrid hepatocyte phenotypes in models of liver injury and regeneration.

Transcriptomic differences are present between GFP^{low} and GFP^{high} BEC populations but are more subtle relative to those observed between GFP^{sub} and GFP^{low/high} populations. Interestingly, we find that GFP^{low} BECs express significantly higher levels of *Krt19*, a pan-biliary marker that has been associated with BEC maturation in induced pluripotent stem cell models.⁴⁵ However, it is unclear whether differential *Krt19* expression in vivo is indicative of different stages of hierarchical cell fate or simply heterogeneity across distinct, mature cell types. Our RNA-seq analysis also uncovered *Wnt7a* and *Wnt7b*, which were recently described as specific to a subpopulation of BECs in a DDC damage model, as uniquely enriched in GFP^{low} cells.⁶ Although we did not detect a significant difference in a previously published Yap gene signature between GFP^{low} and GFP^{high} populations, we observed increased expression of *Cyr61* and *Hes1* in GFP^{high} vs GFP^{low} BECs by RT-qPCR.²¹ *Cyr61* and *Hes1* have previously been identified as Yap-regulated markers of BEC heterogeneity.⁶ Taken in context of our verteporfin experiments demonstrating dependence of Sox9 expression on Yap signaling in organoids, these results suggest that high levels of Sox9^{EGFP} expression in BECs are associated with increased Yap activity.

In organoid-forming assays using medium conditions developed for biliary organoids, both GFP^{low} and GFP^{high} BECs behaved similarly in terms of organoid size and survival.²⁸ It is known that despite heterogeneous Yap activity in vivo, BEC media conditions drive broad activation of Yap in vitro, which could lead to homogenization of organoid phenotypes.⁶ Compellingly, we find that TNF α media conditions result in organoid size differences between GFP^{low}- and GFP^{high}-derived organoids, as well as increased initial organoid formation from GFP^{high} cells. This may indicate that exogenous factors drive or repress functional heterogeneity in BECs. Like GFP^{sub} cells, GFP^{low} and GFP^{high} cells also demonstrated differential activation of HNF4A in TNF α media. Interestingly, GFP^{high}-derived organoids were more likely to express HNF4A, tempting speculation that different subpopulations of BECs may be more likely to undergo transdifferentiation to hepatocytes. Because organoid culture conditions impact multiple signaling pathways and fail to perfectly recapitulate the in vivo environment, further work will be required to expand insight into how in vitro conditions affect BEC subpopulations.

BEC heterogeneity has been classically defined relative to cell size, with small cholangiocytes residing in small ducts and large cholangiocytes residing in large ducts.⁵ In this study, we classified ductules as biliary structures with an inner diameter <10 μ m and ducts as \geq 10 μ m, as defined in recent three-dimensional studies of ductal morphology.²

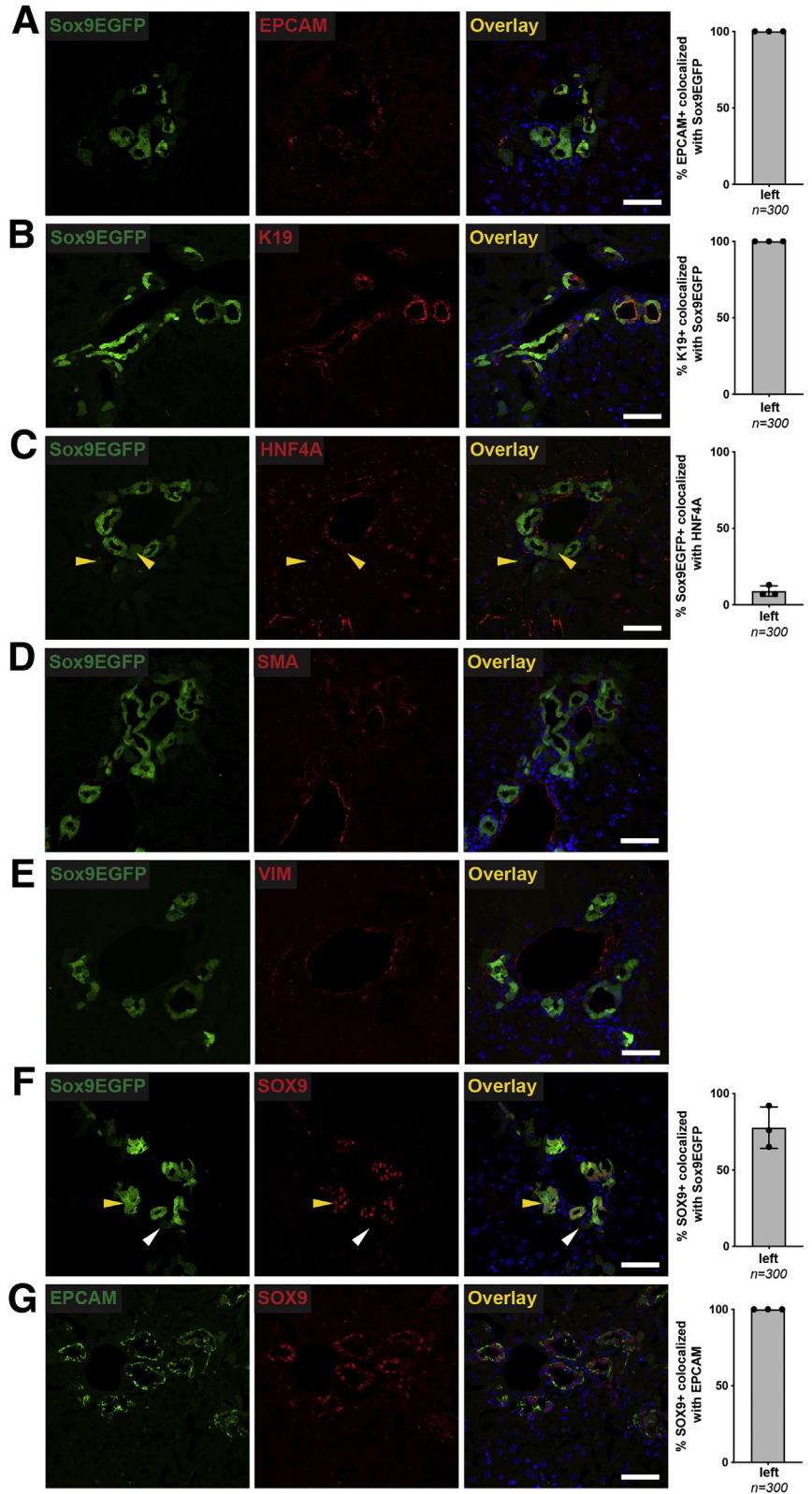


Figure 15. Sox9^{EGFP} expression labels BECs and peribiliary hepatocytes in cholestatic injury after BDL. Immunofluorescence 7 days after BDL demonstrates that all (A) EPCAM⁺ and (B) K19⁺ BECs associated with typical ductular reactions co-express EGFP. (C) Consistent with results in uninjured livers, HNF4A is found in a subpopulation of Sox9^{EGFP}+ peribiliary hepatocytes after BDL (*yellow arrowheads* indicate EGFP⁺/HNF4A⁺). BDL does not result in Sox9^{EGFP} activation in (D) SMA⁺ or (E) VIM⁺ cells. (F) Although some Sox9^{EGFP}+ cells do not express SOX9 after BDL (*white arrowhead*), those with ductal morphology appear SOX9⁺ (*yellow arrowhead*). (G) Independent co-localization of SOX9⁺ with EPCAM indicates that all BECs co-express SOX9 7 days after BDL (n = 100 cells from left lobes of each of 3 biological replicates per co-localization study; scale bars = 50 μm).

Although we demonstrate that GFP^{high} BEC numbers are greater in small ductules relative to larger ducts, our data also show that GFP^{high} BECs in ducts are significantly larger than those in ductules. Together, this suggests that the GFP^{high} population consists of BECs that could be classified as small or large cholangiocytes by classical definitions. Although we do not observe size differences in GFP^{low} BECs located in ductules vs ducts, it is possible that such heterogeneity exists between these smaller structures and rare large ducts leading to the extrahepatic biliary tree, which were not specifically examined in the current study because of their relative scarcity in histologic sections. Future studies may benefit from small cytoplasmic RNA-seq to further tease apart heterogeneity within Sox9^{EGFP} populations. However, the lack of distinct clustering in BEC small cytoplasmic RNA-seq by t-Distributed Stochastic Neighbor Embedding suggests that deep sequencing would be required to detect differences between subpopulations driven by low-expressed genes.^{6,31} Our organoid studies, which demonstrate increased HNF4A protein expression despite no change in *Hnf4a* gene expression, suggest that post-transcriptional regulation may significantly impact biliary identity. Along with our observation that some BECs are SOX9-, this result points to the potential of proteomic characterization to further resolve BEC heterogeneity. We also show that interpopulation differences in organoid size and survival are found in TNF α media conditions but not in BEC media. This suggests that BEC functional heterogeneity, which may be associated with dynamic transcriptomic and proteomic heterogeneity, could be context-dependent and driven by changes to the biliary "niche". The Sox9^{EGFP} model presented here will provide a platform for further exploration of such heterogeneity in biliary homeostasis, injury, and regeneration.

Methods

Mice

Sox9^{EGFP} mice were previously developed and characterized.^{8,46} All Sox9^{EGFP} mice were heterozygous for the EGFP transgene and maintained on the C57Bl/6 background. All experiments were carried out on mice between 8 and 24 weeks of age. Male mice were used for gene expression studies, and male and female mice were used for immunofluorescence and organoid experiments. Mice were fed Tekland Global Soy Protein-Free Extruded Rodent Diet (Envigo, Indianapolis, IN; 2020SX) and received water ad libitum. For gene expression studies, mice were fasted overnight (12–14 hours) before tissue harvest. For in vivo DCA administration, male C57Bl/6 mice were given 24.4 mg/kg DCA in phosphate-buffered saline (PBS) (pH 7.4) or PBS only via a single intraperitoneal injection, as previously described.³⁷ DCA- and vehicle-treated mice were fasted 16 hours and euthanized 24 hours after treatment. Sox9^{EGFP} mice were phenotyped by observing EGFP expression in tail clippings by epifluorescent microscopy.⁸ The Institutional Animal Care and Use Committees of the University of North Carolina at Chapel Hill and Emory University reviewed and approved all animal use protocols.

Bile Duct Ligation

BDLs were carried out by the UNC Animal Surgery Core and the Emory University Pediatric Animal Physiology Core in accordance with Institutional Animal Care and Use Committee approvals, as previously described.⁴⁷ Briefly, 8- to 24-week-old Sox9^{EGFP} mice were anesthetized with 1%–3% isoflurane in 100% oxygen and subjected to ~2-cm midline laparotomy using sterile surgical scissors. The common bile duct was exposed by gentle lifting of liver and caudal movement of the gut by using a sterile swab moistened with sterile 0.9% sodium chloride. The common bile duct was dissected from the portal vein using microserrated forceps and ligated with nonabsorbable 5-0 polyester suture, with a second cranial ligation placed in the same manner to thoroughly occlude the duct. The peritoneal cavity was rinsed with sterile 0.9% sodium before closing the peritoneum and skin with separate running sutures (6-0 monofilament, nonabsorbable). Sham-operated mice underwent the same procedure without ligation of the common bile duct. BDL and sham mice were allowed to recover on heating pads and monitored twice daily for 2 days after surgery and then once daily for the remainder of the study. No adverse effects or unexpected mortality were observed in either group. Analgesia consisted of 0.1 mg/kg buprenorphine given once perioperatively and twice daily postoperatively for 2 days after surgery. Mice were euthanized 7 days after BDL, and livers were processed for histology by intracardiac perfusion of 4% paraformaldehyde (PFA) in PBS, as described below.

Immunofluorescence

Livers were fixed by intracardiac perfusion of 4% PFA in PBS, followed by incubation overnight in 4% PFA in PBS at 4°C. Tissue was transferred to 30% sucrose and incubated overnight at 4°C. Livers were dissected into individual lobes, embedded in Tissue-Tek Optimal Cutting Temperature media (Sakura Finetek USA, Torrance, CA), frozen, and cut into 10- μ m sections. Sections were stored at -80°C until use.

Immunofluorescence was carried out as previously described, and all steps were carried out at room temperature unless otherwise noted.⁹ Sections were permeabilized with 0.3% Triton X-100 in PBS for 20 minutes and then blocked in 1X Animal-Free Blocking Solution (Cell Signaling Technology, Danvers, MA; 15019) for 30 minutes. Primary antibodies were applied in PBS for 2 hours at room temperature or overnight at 4°C. Slides were rinsed in PBS 3 times for 5 minutes. Secondary antibodies were applied in PBS for 45 minutes, and slides were rinsed in PBS 3 times for 5 minutes. Nuclei were stained with bisbenzimidazole (Sigma-Aldrich; B2883), diluted 1:1000 in PBS for 10 minutes, before a final wash in PBS 3 times for 5 minutes. Slides were mounted to coverslips using Hydromount Mounting Media (Electron Microscopy Sciences, Hatfield, PA; 17966). For semiquantitative confocal analysis of EGFP, slides were mounted using ProLong Gold Mounting Media (Thermo Fisher, Waltham, MA; P36934). For mouse-on-mouse detection, tissue sections were incubated in 0.13 mg/mL goat anti-mouse Fab fragments for 1 hour at room

temperature or overnight at 4°C immediately before primary antibody incubation. Antibodies used in this article are listed in [Supplementary Table 4](#). For co-labeling with WGA, tissue was incubated for 10 minutes in 1 mg/mL WGA-AlexaFluor647 (Thermo Fisher; W32466) in Hanks' balanced salt solution before permeabilization. After WGA incubation, tissue was washed in Hanks' balanced salt solution twice for 5 minutes.

Images were acquired by using an Olympus IX-81 (Tokyo, Japan) widefield epifluorescent microscope or Zeiss LSM700 (Carl Zeiss, Oberkochen, Germany) and Leica SP8 (Wetzlar, Germany) confocal microscopes. Confocal images of tissue were acquired as 1 μ mol/L optical sections; confocal images of organoids were acquired as 5 μ mol/L optical sections. Low magnification image of Sox9^{EGFP} right lobe ([Figure 1A](#)) was acquired by tile scan imaging of fresh tissue immediately after dissection by using Olympus IX-81 widefield epifluorescent microscope fitted with 4 \times objective lens. Tile scanned images were merged by image stitching in Metamorph (Molecular Devices, San Jose, CA). Confocal imaging was carried out in the Microscopy Services Laboratory at UNC Chapel Hill and the Integrated Cellular Imaging Core at Emory University. Quantification of confocal images was carried out in ImageJ (National Institutes of Health, Bethesda, MA) with subtraction of background fluorescence. Statistical analyses were carried out in Prism 8.4.2 (GraphPad Software, San Diego, CA).

Intrahepatic Bile Duct Isolation

To isolate single BECs from intrahepatic bile ducts, we dissociated liver tissue as previously described with minor modifications.¹⁸ Briefly, liver lobes were dissected without removing extrahepatic duct and gallbladder to avoid contamination of intrahepatic biliary preps with extrahepatic biliary tissue. The tissue was rinsed in sterile Dulbecco PBS (Gibco, Gaithersburg, MD), minced (<0.5 cm² pieces) with a razor blade, and transferred to 50-mL conical tube. Liver tissue pieces were rinsed twice with Liver Wash Buffer (DMEM-H [Gibco], 1% fetal bovine serum, 1% Glutamax [Gibco], 1% penicillin/streptomycin [Gibco]) by resuspending and allowing tissue to sediment before removing supernatant. After the second rinse, tissue was centrifuged at 600g at 4°C for 5 minutes to remove residual Liver Wash Buffer. The supernatant was discarded, and liver tissue pieces were resuspended in 10 mL of Dissociation buffer (Liver Wash Buffer with 0.15 mg/mL collagenase type XI [Sigma-Aldrich, St Louis, MO; C9407], 0.3 U/mL Dispase [Corning, Corning, NY; 354235], 200 μ g/mL DNase [Sigma-Aldrich; DN25]), pre-warmed to 37°C. The tube was transferred to a rocking platform (60 rpm) and incubated at 37°C for 90 minutes with continuous shaking. The tube was retrieved every 30 minutes and vigorously pipetted 50 times using a P1000 micropipette set to 1 mL to aid in dissociation of bile ducts. After 90 minutes of digest, dissociated tissue was rinsed twice with 10 mL Liver Wash Buffer, followed by centrifugation at 200g at 4°C for 5 minutes. Supernatant was discarded after each wash by careful decanting so as not to disturb the cell pellet. The pellet was

resuspended in 5 mL Red Blood Cell Lysis Buffer (BioLegend, San Jose, CA; 420301) diluted in sterile Molecular Grade Water (Corning), as per manufacturer protocol, and incubated on ice for 5 minutes with repeated agitation. Ten milliliters Dulbecco PBS (Gibco) was added to quench the lysis buffer, and the tube was centrifuged at 600g at 4°C for 5 minutes. Supernatant was discarded, and ductal fragments were resuspended in 500 μ L Advanced Dulbecco modified Eagle medium (DMEM) (Gibco) for whole duct organoid culture or used for single cell dissociation.

Single BEC Dissociation and Flow Cytometry/FACS

Ductal fragments were resuspended in 1 mL TrypLE (Gibco) with 100 μ g/mL Y-27632 (Selleck Chemicals, Houston, TX; S1049) for single cell dissociation. The tube was incubated at 37°C for 12 minutes with vigorous pipetting every 2 minutes to aid in dissociation of isolated ductal fragments. Ten milliliters Advanced DMEM (Gibco) was added to quench the TrypLE and stop the dissociation. Dissociated cells were passed through a 40- μ m cell strainer into a new 50-mL conical tube and centrifuged at 600g at 4°C for 5 minutes. The supernatant was discarded, and cells were resuspended in 500 μ L Sort Media (Advanced DMEM with 500 μ L B27 supplement without vitamin A [Thermo Fisher], 250 μ L N2 supplement [Thermo Fisher], 250 μ L Glutamax [Gibco], 250 μ L Hepes Buffer Solution [Gibco], 250 μ L penicillin/streptomycin [Gibco], 0.1% Y-27632 100 μ L/mL [Selleck Chemicals; S1049], 0.1% DNase [Sigma-Aldrich; DN25]).

Single BECs were stained with anti-CD31-APC (1:100) (BioLegend) and anti-CD45-APC (1:100) (BioLegend) and incubated, covered, on ice for 45 minutes. Cells were rinsed with 3 mL Advanced DMEM (Gibco) and centrifuged at 600g at 4°C for 5 minutes. After decanting the supernatant, the cells were resuspended in 1.5 mL Sort Media. Five microliters of 7AAD (BioLegend; 420404) and 5 μ L AnnexinV-APC (BioLegend; 640941) were added to resuspended cells to distinguish dead and dying cells, respectively. Cells were analyzed and collected by using a Sony SH800 fluorescence-activated cell sorter. Gating schemes are shown in [Figures 6A and 13A](#). For gene expression experiments, cells were collected directly into 500 μ L RNA Lysis Buffer (Ambion RNAqueous Micro Kit, Austin, TX; AM1931); for organoid culture experiments, cells were collected directly into Sort Media.

RNA Isolation and RT-qPCR

FACS-isolated cells and organoids for gene expression studies were lysed in RNA Lysis Buffer, and RNA was isolated using the RNAqueous Micro Kit (Ambion) following manufacturer instructions. cDNA was generated with the iScript cDNA Synthesis Kit (BioRad, Hercules, CA; 1708891) and diluted 1:10 in molecular grade H₂O (Corning) for RT-qPCR. RT-qPCR was carried out using Taqman probes and SsoAdvanced Universal Probes Supermix (BioRad; 1725280). To detect nascent Sox9 RNA, primers were designed spanning the junction of Sox9 exon 2-intron 2

using Primer-BLAST.⁴⁸ Primers were validated to have efficiency between 90% and 110% and produced a single PCR product that was validated by Sanger sequencing (Eurofins Genomics, Luxembourg). RT-qPCR for nascent *Sox9* was carried out using SsoAdvanced Universal SYBR Green Supermix (BioRad; 1725270). Relative fold change of gene expression was calculated using the delta-delta C_T method, with *18S* as the internal reference gene.⁴⁹ Statistical analyses were carried out in Prism 8.4.2 (GraphPad). Taqman assay IDs and *Sox9* primer sequences used in this article are listed in [Supplementary Table 5](#).

RNA-seq and Analysis

Libraries for RNA-seq were prepared as previously described.⁹ Twelve thousand cells per *Sox9*^{EGFP} population were collected directly into 500 μ L RNA Lysis Buffer (Ambion RNAqueous Micro Kit), and RNA was isolated as described above, with an adjustment to the protocol so that final volume of eluate is equivalent to 15 mL. cDNA was prepared from 5 mL RNA, which was used to validate FACS isolation by RT-qPCR for *Egfp* (Life Technologies, Carlsbad, CA) using *18S* as the internal reference gene. One microliter of RNA from each sample was used to assess RNA integrity number by Bioanalyzer (Agilent, Santa Clara, CA) using the RNA Pico assay. RIN values were ≥ 7.0 for all RNA-seq samples. Libraries were prepared from 8 mL RNA using the SMARTer Stranded Total RNA-seq Pico kit v2 (Clontech, Mountain View, CA) per manufacturer instructions. Libraries were pooled in equimolar ratios using concentrations determined by Qubit 3.0 High Sensitivity DNA assay (Life Technologies) and Bioanalyzer (Agilent) using the High Sensitivity DNA Analysis kit. Libraries were sequenced on a NextSeq500 (Illumina, San Diego, CA) with 75 base pair single-end reads, v2 chemistry.

Transcript abundances were estimated using Salmon (1.1.0) indexed to Gencode mouse annotations v24 and collapsed to gene counts using tximport (1.14.2).^{50,51} Differential expression analysis was performed using DESeq2 (1.26.0).⁵² Heatmaps were generated using ComplexHeatmap (2.2.0) and the Z-scored normalized count values. Signature scores were derived using the singscore R package (1.6.0)¹⁹; data.^{20–22} P-values for gene set signature scores are presented in [Supplementary Table 3](#). All code used in these analyses available at <https://doi.org/10.5281/zenodo.3858321>. RNA-seq data are deposited in GEO under series number: GSE151387.

Primary Hepatocyte Isolation

Hepatocyte isolation was adapted from a previously published protocol.⁵³ Briefly, mice weighing 20–35 g were anesthetized with Nembutal (40–60 mg/kg, intraperitoneal). Abdominal cavity was opened, and portal vein was cannulated (24-gauge \times $\frac{3}{4}$ -inch Terumo Surflo ETFE IV catheter; Fisher Scientific, Hampton, NH). The catheter was connected to a perfusion system for cell isolation from mouse organs (Cat #73-3659; Harvard Apparatus, Holliston, MA). Liver was perfused with 50 mL of 37°C sterile buffer I solution (50 mmol/L EGTA, 1 mol/L glucose, 1% penicillin/

streptomycin in calcium- and magnesium-free Hank's balanced salt solution) at a rate of 7 mL/min. At this time, inferior vena cava was cut. Subsequently, liver was digested with 40 mL of 37°C sterile buffer II solution (1 mol/L CaCl_2 , 1 mol/L glucose, 1% penicillin/streptomycin, and 3600 U Collagenase IV in calcium- and magnesium-free Hank's balanced salt solution) at a rate of 5 mL/min. Livers were surgically removed, and hepatocytes were released in cold isolation medium (1X DMEM, 1% penicillin/streptomycin) by removing the Glisson's capsule using sterile tweezers. Hepatocytes were isolated by size exclusion using 100-mm and 70-mm filters, respectively. Cells were washed at 120g for 5 minutes at 4°C. Live/dead cell exclusion was performed by Percoll gradient (1:1 1X Percoll/isolation medium) and centrifugation at 120g for 5 minutes at 4°C. Hepatocytes were resuspended in isolation medium.

Biliary and Hepatocyte Organoid Culture

Whole duct culture and bile acid treatment. Ten microliter aliquots from ductal preps were examined by light microscopy to qualitatively determine cellular density. Five to ten microliters of ductal prep was diluted in Advanced DMEM/F12 (Gibco), and Cultrex Type II Growth Factor Reduced extracellular matrix (R&D Biosystems, Minneapolis, MN; 3533-010-02) was added to a final concentration of 66% Cultrex. Cultrex-duct suspensions were plated as 40- μ L droplets per well in pre-warmed 48-well plates and allowed to polymerize at 37°C for 20 minutes. After polymerization, droplets were overlaid with 200 μ L Biliary Expansion Media (50% Advanced DMEM/F12 [Gibco], 40% WNT3A-conditioned media, 10% RSP01-conditioned media, B27 supplement without vitamin A [Thermo Fisher], N2 supplement [Thermo Fisher], Glutamax [Gibco], 10 mmol/L HEPES [Gibco], penicillin/streptomycin [Gibco], 50 ng/mL recombinant murine EGF [Gibco; PMG8043], 100 ng/mL recombinant human Noggin [Peprotech, Rocky Hill, NJ; 120-10C], 100 ng/mL recombinant human FGF10 [Peprotech; 100-26], 10 μ mol/L recombinant human gastrin [Sigma-Aldrich; G9145], 50 ng/mL recombinant human HGF [Peprotech 100-39H], 10 mmol/L nicotinamide, and 10 μ mol/L Y-27632 [Selleck Chemicals]). Media were replaced every other day. Starting on day 4, WNT3A-conditioned medium was removed and replaced with Advanced DMEM/F12, and Noggin and Y-27632 were withdrawn from culture.

For bile acid and verteporfin organoid experiments, ductal organoids were passaged twice before treatment. Organoids were grown for 7 days before each passage and passaged by removing medium and adding 250 μ L TrypLE (Gibco). Cultrex droplets were mechanically dissociated in TrypLE by pipetting and then incubated at 37°C for 3 minutes. TrypLE was quenched by adding 250 μ L Advanced DMEM/F12, and organoid fragments were pelleted at 6000g for 5 minutes at room temperature. Organoid fragments were re-plated at 1:2 ratio as 40- μ L droplets (66% Cultrex: 34% Advanced DMEM/F12) in pre-warmed 48-well plates, as described above. For monolayer experiments, organoid fragments were passaged onto 48-well plates coated with

10% Cultrex at passage 2. After each passage, organoids and monolayers were initially grown in Biliary Expansion Media with WNT3A, Noggin, and Y27632 for 4 days. WNT3A, Noggin, and Y27632 were removed from culture for 48 hours before treatment. Samples were treated with 50 $\mu\text{mol/L}$ deoxycholic acid (Sigma-Aldrich), 1 $\mu\text{mol/L}$ verteporfin (Tocris Bioscience, Bristol, UK; 5305), or an equivalent volume of dimethyl sulfoxide for 24 hours before lysis in 500 μL of RNA Lysis Buffer (Ambion RNAqueous Micro Kit). To determine bile acid presence in organoid lumens, organoids were treated with 50 $\mu\text{mol/L}$ FITC-conjugated DCA (E. Mash, University of Arizona) or 40 kDa FITC-conjugated dextran (Sigma-Aldrich; FD40S).⁵⁴ Organoid images were acquired as 1 $\mu\text{mol/L}$ optical sections on a Zeiss LSM700 confocal microscope 9 hours after treatment with DCA or dextran.

Single cell culture. FACS-isolated BECs were resuspended in Cultrex Type II Growth Factor Reduced extracellular matrix (R&D Biosystems). For organoid survival and whole-mount immunofluorescence experiments, Cultrex cell suspensions were plated as 40- μL droplets per well in pre-warmed 48-well plates. For gene expression experiments, Cultrex cell suspensions were plated as 10- μL droplets per well to pre-warmed 96-well plates. All Cultrex droplets were allowed to polymerize at 37°C for 20 minutes. After polymerization, BEC or TNF α medium was overlaid: 200 μL per well for 48-well plates or 100 μL per well for 96-well plates. BECs were plated at density of 5000 cells per 40- μL Cultrex droplet per well (48-well plate) or 1200 cells per 10- μL Cultrex droplet per well (96-well plate). Primary hepatocytes were plated at a density of 10,000 cells per 40- μL Cultrex droplet per well (48-well plate).

Organoids grown in BEC media were initially overlaid with Biliary Expansion Media. Medium was replaced every other day. Starting on day 4, WNT3A-conditioned medium was removed and replaced with Advanced DMEM/F12, and Noggin and Y-27632 were withdrawn from culture. Organoids grown in TNF α conditions were overlaid with TNF α media (Advanced DMEM/F12 [Gibco], B27 supplement without vitamin A [Thermo Fisher], N2 supplement [Thermo Fisher], Glutamax [Gibco], 10 mmol/L HEPES [Gibco], penicillin/streptomycin [Gibco], 25 ng/mL recombinant murine EGF [Gibco], 50 ng/mL recombinant human HGF [Peprotech], 10 $\mu\text{mol/L}$ Y-27632 [Selleck Chemicals], 1 $\mu\text{mol/L}$ A8301 [Tocris; 2939], 3 $\mu\text{mol/L}$ CHIR99021 [Selleck Chemicals; S1263], and 100 ng/mL recombinant murine TNF α [Peprotech; 315-01A]). Medium was replaced every other day.

Whole Mount Immunofluorescence

Organoids grown from single cells were fixed 7 days after plating as follows. All steps were carried out at room temperature unless noted. Overlay medium was removed, and 200 μL of 4% paraformaldehyde (VWR 41678) in Dulbecco PBS (pre-warmed at 37°C) was added to each well for 15 minutes to fix the organoids. Four percent paraformaldehyde was removed, and the organoids were rinsed with 200 μL PBS (Gibco) twice for 5 minutes. The organoids

were permeabilized with 200 μL 0.5% Triton (Sigma-Aldrich; T8787) in PBS for 20 minutes and then rinsed with 200 μL 100 mmol/L glycine in PBS twice for 15 minutes. Organoids were incubated with 250 μL of Blocking Buffer (10% Normal Donkey Serum [Jackson ImmunoResearch Laboratories, West Grove, PA; 017-000-121] in Immunofluorescence Buffer [Dulbecco PBS- 0.1% bovine serum albumin, 0.2% Triton, 0.05% Tween-20]) for 90 minutes. Primary antibodies were applied in 250 μL of Blocking Buffer and incubated overnight at 4°C.

Primary antibodies were removed, and organoids were washed with 250 μL Immunofluorescence Buffer 3 times for 20 minutes. Secondary antibodies were applied in 250 μL of Blocking Buffer and incubated for 2 hours. Secondary antibodies were removed, and organoids were washed with 250 μL Immunofluorescence Buffer 3 times for 20 minutes. Nuclei were stained with bisbenzimidazole (Sigma-Aldrich) diluted 1:1000 in Immunofluorescence Buffer for 30 minutes. Organoids were washed with Dulbecco PBS for 5 minutes 3 times and immediately quantified. SOX9 and HNF4A expression was observed by using an Olympus IX-81 inverted epifluorescent microscope.

Supplementary Data

Note: to access the supplementary materials accompanying this article, visit the online version of *Cellular and Molecular Gastroenterology and Hepatology* at www.cmhjournal.org.

References

1. Maroni L, Haibo B, Ray D, Zhou T, Wan Y, Meng F, Marziani M, Alpini G. Functional and structural features of cholangiocytes in health and disease. *Cell Mol Gastroenterol Hepatol* 2015;1:368–380.
2. Kamimoto K, Kaneko K, Kok CY, Okada H, Miyajima A, Itoh T. Heterogeneity and stochastic growth regulation of biliary epithelial cells dictate dynamic epithelial tissue remodeling. *Elife* 2016;5.
3. Manco R, Clerbaux LA, Verhulst S, Bou Nader M, Sempoux C, Ambroise J, Bearzatto B, Gala JL, Horsmans Y, van Grunsven L, Desdouets C, Leclercq I. Reactive cholangiocytes differentiate into proliferative hepatocytes with efficient DNA repair in mice with chronic liver injury. *J Hepatol* 2019;70:1180–1191.
4. Raven A, Lu WY, Man TY, Ferreira-Gonzalez S, O'Duibhir E, Dwyer BJ, Thomson JP, Meehan RR, Bogorad R, Koteliensky V, Kotelevtsev Y, Ffrench-Constant C, Boulter L, Forbes SJ. Cholangiocytes act as facultative liver stem cells during impaired hepatocyte regeneration. *Nature* 2017;547:350–354.
5. Alpini G, Roberts S, Kuntz SM, Ueno Y, Gubba S, Podila PV, LeSage G, LaRusso NF. Morphological, molecular, and functional heterogeneity of cholangiocytes from normal rat liver. *Gastroenterology* 1996;110:1636–1643.
6. Pepe-Mooney BJ, Dill MT, Alemany A, Ordovas-Montanes J, Matsushita Y, Rao A, Sen A, Miyazaki M, Anakk S, Dawson PA, Ono N, Shalek AK, van Oudenaarden A, Camargo FD. Single-cell analysis of the liver epithelium reveals dynamic heterogeneity and an

- essential role for YAP in homeostasis and regeneration. *Cell Stem Cell* 2019.
7. Yimlamai D, Christodoulou C, Galli GG, Yanger K, Pepe-Mooney B, Gurung B, Shrestha K, Cahan P, Stanger BZ, Camargo FD. Hippo pathway activity influences liver cell fate. *Cell* 2014;157:1324–1338.
 8. Formeister EJ, Sionas AL, Lorange DK, Barkley CL, Lee GH, Magness ST. Distinct SOX9 levels differentially mark stem/progenitor populations and enteroendocrine cells of the small intestine epithelium. *Am J Physiol Gastrointest Liver Physiol* 2009;296:G1108–G1118.
 9. Raab JR, Tulasi DY, Wager KE, Morowitz JM, Magness ST, Gracz AD. Quantitative classification of chromatin dynamics reveals regulators of intestinal stem cell differentiation. *Development* 2020;147(1).
 10. Ramalingam S, Daughtridge GW, Johnston MJ, Gracz AD, Magness ST. Distinct levels of Sox9 expression mark colon epithelial stem cells that form colonoids in culture. *Am J Physiol Gastrointest Liver Physiol* 2012;302:G10–G20.
 11. Antoniou A, Raynaud P, Cordi S, Zong Y, Tronche F, Stanger BZ, Jacquemin P, Pierreux CE, Clotman F, Lemaigre FP. Intrahepatic bile ducts develop according to a new mode of tubulogenesis regulated by the transcription factor SOX9. *Gastroenterology* 2009;136:2325–2333.
 12. Cardinale V, Wang Y, Carpino G, Cui CB, Gatto M, Rossi M, Berloco PB, Cantafora A, Wauthier E, Furth ME, Inverardi L, Dominguez-Bendala J, Ricordi C, Gerber D, Gaudio E, Alvaro D, Reid L. Multipotent stem/progenitor cells in human biliary tree give rise to hepatocytes, cholangiocytes, and pancreatic islets. *Hepatology* 2011;54:2159–2172.
 13. Rimland CA, Tilson SG, Morell CM, Tomaz RA, Lu WY, Adams SE, Georgakopoulos N, Otaizo-Carrasquero F, Myers TG, Ferdinand JR, Gieseck RL 3rd, Sampaziotis F, Tysoe OC, Wesley B, Muraro D, Oniscu GC, Hannan NR, Forbes SJ, Saeb-Parsy K, Wynn TA, Vallier L. Regional differences in human biliary tissues and corresponding in vitro derived organoids. *Hepatology* 2020.
 14. Zong Y, Stanger BZ. Molecular mechanisms of liver and bile duct development. *Wiley Interdiscip Rev Dev Biol* 2012;1:643–655.
 15. Font-Burgada J, Shalapour S, Ramaswamy S, Hsueh B, Rossell D, Umemura A, Taniguchi K, Nakagawa H, Valasek MA, Ye L, Kopp JL, Sander M, Carter H, Deisseroth K, Verma IM, Karin M. Hybrid periportal hepatocytes regenerate the injured liver without giving rise to cancer. *Cell* 2015;162:766–779.
 16. Troeger JS, Mederacke I, Gwak GY, Dapito DH, Mu X, Hsu CC, Pradere JP, Friedman RA, Schwabe RF. Deactivation of hepatic stellate cells during liver fibrosis resolution in mice. *Gastroenterology* 2012;143:1073–1083 e22.
 17. Glaser SS, Gaudio E, Rao A, Pierce LM, Onori P, Franchitto A, Francis HL, Dostal DE, Venter JK, DeMorrow S, Mancinelli R, Carpino G, Alvaro D, Kopriva SE, Savage JM, Alpini GD. Morphological and functional heterogeneity of the mouse intrahepatic biliary epithelium. *Lab Invest* 2009;89:456–469.
 18. Broutier L, Andersson-Rolf A, Hindley CJ, Boj SF, Clevers H, Koo BK, Huch M. Culture and establishment of self-renewing human and mouse adult liver and pancreas 3D organoids and their genetic manipulation. *Nat Protoc* 2016;11:1724–1743.
 19. Foroutan M, Bhuvu DD, Lyu R, Horan K, Cursons J, Davis MJ. Single sample scoring of molecular phenotypes. *BMC Bioinformatics* 2018;19:404.
 20. Schaub JR, Huppert KA, Kurial SNT, Hsu BY, Cast AE, Donnelly B, Karns RA, Chen F, Rezvani M, Luu HY, Mattis AN, Rougemont AL, Rosenthal P, Huppert SS, Willenbring H. De novo formation of the biliary system by TGFbeta-mediated hepatocyte transdifferentiation. *Nature* 2018;557:247–251.
 21. Dong J, Feldmann G, Huang J, Wu S, Zhang N, Comerford SA, Gayyed MF, Anders RA, Maitra A, Pan D. Elucidation of a universal size-control mechanism in *Drosophila* and mammals. *Cell* 2007;130:1120–1133.
 22. Villanueva A, Alsinet C, Yanger K, Hoshida Y, Zong Y, Toffanin S, Rodriguez-Carunchio L, Sole M, Thung S, Stanger BZ, Llovet JM. Notch signaling is activated in human hepatocellular carcinoma and induces tumor formation in mice. *Gastroenterology* 2012;143:1660–1669 e7.
 23. Halpern KB, Shenhav R, Massalha H, Toth B, Egozi A, Massasa EE, Medgalia C, David E, Giladi A, Moor AE, Porat Z, Amit I, Itzkovitz S. Paired-cell sequencing enables spatial gene expression mapping of liver endothelial cells. *Nat Biotechnol* 2018;36:962–970.
 24. DeLeve LD, Wang X, Hu L, McCuskey MK, McCuskey RS. Rat liver sinusoidal endothelial cell phenotype is maintained by paracrine and autocrine regulation. *Am J Physiol Gastrointest Liver Physiol* 2004;287:G757–G763.
 25. Mederacke I, Hsu CC, Troeger JS, Huebener P, Mu X, Dapito DH, Pradere JP, Schwabe RF. Fate tracing reveals hepatic stellate cells as dominant contributors to liver fibrosis independent of its aetiology. *Nat Commun* 2013;4:2823.
 26. Ayyaz A, Kumar S, Sangiorgi B, Ghoshal B, Gosio J, Ouladan S, Fink M, Barutcu S, Trcka D, Shen J, Chan K, Wrana JL, Gregorieff A. Single-cell transcriptomes of the regenerating intestine reveal a revival stem cell. *Nature* 2019;569:121–125.
 27. Poling HM, Mohanty SK, Tiao GM, Huppert SS. A comprehensive analysis of aquaporin and secretory related gene expression in neonate and adult cholangiocytes. *Gene Expr Patterns* 2014;15:96–103.
 28. Huch M, Dorrell C, Boj SF, van Es JH, Li VS, van de Wetering M, Sato T, Hamer K, Sasaki N, Finegold MJ, Haft A, Vries RG, Grompe M, Clevers H. In vitro expansion of single Lgr5+ liver stem cells induced by Wnt-driven regeneration. *Nature* 2013;494:247–250.
 29. Peng WC, Logan CY, Fish M, Anbarchian T, Aguisanda F, Alvarez-Varela A, Wu P, Jin Y, Zhu J, Li B, Grompe M, Wang B, Nusse R. Inflammatory cytokine TNFalpha promotes the long-term expansion of primary hepatocytes in 3D culture. *Cell* 2018;175:1607–1619 e15.

30. Aloia L, McKie MA, Vernaz G, Cordero-Espinoza L, Aleksieva N, van den Amele J, Antonica F, Font-Cunill B, Raven A, Aiese Cigliano R, Belenguer G, Mort RL, Brand AH, Zernicka-Goetz M, Forbes SJ, Miska EA, Huch M. Epigenetic remodelling licences adult cholangiocytes for organoid formation and liver regeneration. *Nature Cell Biology* 2019;21:1321–1333.
31. Planas-Paz L, Sun T, Pikiolak M, Cochran NR, Bergling S, Orsini V, Yang Z, Sigoillot F, Jetzer J, Syed M, Neri M, Schuierer S, Morelli L, Hoppe PS, Schwarzer W, Cobos CM, Alford JL, Zhang L, Cuttat R, Waldt A, Carballido-Perrig N, Nigsch F, Kinzel B, Nicholson TB, Yang Y, Mao X, Terracciano LM, Russ C, Reece-Hoyes JS, Gubser Keller C, Sailer AW, Bouwmeester T, Greenbaum LE, Lugus JJ, Cong F, McAllister G, Hoffman GR, Roma G, Tchorz JS. YAP, but not RSPO-LGR4/5, signaling in biliary epithelial cells promotes a ductular reaction in response to liver injury. *Cell Stem Cell* 2019;25:39–53 e10.
32. Hu H, Gehart H, Artegiani B, C LO-I, Dekkers F, Basak O, van Es J, Chuva de Sousa Lopes SM, Begthel H, Korving J, van den Born M, Zou C, Quirk C, Chiriboga L, Rice CM, Ma S, Rios A, Peters PJ, de Jong YP, Clevers H. Long-term expansion of functional mouse and human hepatocytes as 3D organoids. *Cell* 2018;175:1591–1606 e19.
33. Song S, Ajani JA, Honjo S, Maru DM, Chen Q, Scott AW, Heallen TR, Xiao L, Hofstetter WL, Weston B, Lee JH, Wadhwa R, Sudo K, Stroehlein JR, Martin JF, Hung MC, Johnson RL. Hippo coactivator YAP1 upregulates SOX9 and endows esophageal cancer cells with stem-like properties. *Cancer Res* 2014;74:4170–4182.
34. Yi J, Lu L, Yanger K, Wang W, Sohn BH, Stanger BZ, Zhang M, Martin JF, Ajani JA, Chen J, Lee JS, Song S, Johnson RL. Large tumor suppressor homologs 1 and 2 regulate mouse liver progenitor cell proliferation and maturation through antagonism of the coactivators YAP and TAZ. *Hepatology* 2016;64:1757–1772.
35. Liu-Chittenden Y, Huang B, Shim JS, Chen Q, Lee SJ, Anders RA, Liu JO, Pan D. Genetic and pharmacological disruption of the TEAD-YAP complex suppresses the oncogenic activity of YAP. *Genes Dev* 2012;26:1300–1305.
36. Anakk S, Bhosale M, Schmidt VA, Johnson RL, Finegold MJ, Moore DD. Bile acids activate YAP to promote liver carcinogenesis. *Cell Rep* 2013;5:1060–1069.
37. Paolini M, Pozzetti L, Montagnani M, Potenza G, Sabatini L, Antelli A, Cantelli-Forti G, Roda A. Ursodeoxycholic acid (UDCA) prevents DCA effects on male mouse liver via up-regulation of CYP [correction of CXP] and preservation of BSEP activities. *Hepatology* 2002;36:305–314.
38. Thomas AM, Hart SN, Kong B, Fang J, Zhong XB, Guo GL. Genome-wide tissue-specific farnesoid X receptor binding in mouse liver and intestine. *Hepatology* 2010;51:1410–1419.
39. Dai J, Wang H, Dong Y, Zhang Y, Wang J. Bile acids affect the growth of human cholangiocarcinoma via NF- κ B pathway. *Cancer Invest* 2013;31:111–120.
40. Gadd VL, Aleksieva N, Forbes SJ. Epithelial plasticity during liver injury and regeneration. *Cell Stem Cell* 2020;27:557–573.
41. Yanger K, Zong Y, Maggs LR, Shapira SN, Maddipati R, Aiello NM, Thung SN, Wells RG, Greenbaum LE, Stanger BZ. Robust cellular reprogramming occurs spontaneously during liver regeneration. *Genes Dev* 2013;27:719–724.
42. Athwal VS, Pritchett J, Llewellyn J, Martin K, Camacho E, Raza SM, Phythian-Adams A, Birchall LJ, Mullan AF, Su K, Pearmain L, Dolman G, Zaitoun AM, Friedman SL, MacDonald A, Irving WL, Guha IN, Hanley NA, Piper Hanley K. SOX9 predicts progression toward cirrhosis in patients while its loss protects against liver fibrosis. *EMBO Mol Med* 2017;9:1696–1710.
43. Hanley KP, Oakley F, Sugden S, Wilson DI, Mann DA, Hanley NA. Ectopic SOX9 mediates extracellular matrix deposition characteristic of organ fibrosis. *J Biol Chem* 2008;283:14063–14071.
44. Rezanejad H, Ouziel-Yahalom L, Keyzer CA, Sullivan BA, Hollister-Lock J, Li WC, Guo L, Deng S, Lei J, Markmann J, Bonner-Weir S. Heterogeneity of SOX9 and HNF1beta in pancreatic ducts is dynamic. *Stem Cell Reports* 2018;10:725–738.
45. Sampaziotis F, de Brito MC, Madrigal P, Bertero A, Saeb-Parsy K, Soares FAC, Schrupf E, Melum E, Karlsen TH, Bradley JA, Gelson WT, Davies S, Baker A, Kaser A, Alexander GJ, Hannan NRF, Vallier L. Cholangiocytes derived from human induced pluripotent stem cells for disease modeling and drug validation. *Nat Biotechnol* 2015;33:845–852.
46. Gong S, Zheng C, Doughty ML, Losos K, Didkovsky N, Schambra UB, Nowak NJ, Joyner A, Leblanc G, Hatten ME, Heintz N. A gene expression atlas of the central nervous system based on bacterial artificial chromosomes. *Nature* 2003;425:917–925.
47. Tag CG, Sauer-Lehnen S, Weiskirchen S, Borkham-Kamphorst E, Tolba RH, Tacke F, Weiskirchen R. Bile duct ligation in mice: induction of inflammatory liver injury and fibrosis by obstructive cholestasis. *J Vis Exp* 2015;96:52438.
48. Ye J, Coulouris G, Zaretskaya I, Cutcutache I, Rozen S, Madden TL. Primer-BLAST: a tool to design target-specific primers for polymerase chain reaction. *BMC Bioinformatics* 2012;13:134.
49. Pfaffl MW. A new mathematical model for relative quantification in real-time RT-PCR. *Nucleic Acids Res* 2001;29:e45.
50. Patro R, Duggal G, Love MI, Irizarry RA, Kingsford C. Salmon provides fast and bias-aware quantification of transcript expression. *Nat Methods* 2017;14:417–419.
51. Sonesson C, Love MI, Robinson MD. Differential analyses for RNA-seq: transcript-level estimates improve gene-level inferences. *F1000Res* 2015;4:1521.
52. Love MI, Huber W, Anders S. Moderated estimation of fold change and dispersion for RNA-seq data with DESeq2. *Genome Biol* 2014;15:550.

53. Kim ND, Moon JO, Slitt AL, Copples BL. Early growth response factor-1 is critical for cholestatic liver injury. *Toxicol Sci* 2006;90:586–595.
54. Jean-Louis S, Akare S, Ali MA, Mash EA Jr, Meuillet E, Martinez JD. Deoxycholic acid induces intracellular signaling through membrane perturbations. *J Biol Chem* 2006;281:14948–14960.

Diego Martinez Castaneda (Formal analysis: Supporting; Investigation: Supporting; Visualization: Supporting; Writing – review & editing: Supporting)
 Kortney Wager (Formal analysis: Supporting; Investigation: Supporting; Methodology: Supporting; Visualization: Supporting)
 Connor B. Hogan (Formal analysis: Supporting; Investigation: Supporting)
 Karel P. Alcedo (Investigation: Supporting; Methodology: Supporting; Writing – review & editing: Supporting)
 Jesse R. Raab (Formal analysis: Supporting; Investigation: Supporting; Visualization: Supporting; Writing – review & editing: Supporting)
 Adam David Gracz, PhD (Conceptualization: Lead; Data curation: Lead; Formal analysis: Equal; Funding acquisition: Lead; Investigation: Equal; Methodology: Equal; Project administration: Lead; Supervision: Lead; Validation: Equal; Visualization: Equal; Writing – original draft: Lead; Writing – review & editing: Lead)

Received July 28, 2020. Accepted January 13, 2021.

Correspondence

Address correspondence to: Adam D. Gracz, PhD, 615 Michael Street NE, Suite 201A, Atlanta, Georgia 30322. e-mail: agracz@emory.edu; fax: (404) 727-5767.

Acknowledgments

The authors thank Drs Bailey Zwarcyz, Scott Magness, Susan Henning, Paul Dawson, and Terry Magnuson and members of the Magnuson Lab (UNC) for helpful discussion and feedback. FITC-DCA was a gift of Dr Eugene A. Mash (University of Arizona). Dr Joshua Maxwell and Ming Shen provided assistance with bile duct ligation surgery via the Children's Healthcare of Atlanta and Emory University's Pediatric Animal Physiology Core.

ORCID Authorship Contributions

Deepthi Y. Tulasi (Data curation: Equal; Formal analysis: Equal; Investigation: Equal; Visualization: Lead; Writing – review & editing: Supporting)

Conflicts of interest

The authors disclose no conflicts.

Funding

Supported by the American Gastroenterological Association (Research Scholar Award to A.D.G.), the National Institutes of Diabetes and Digestive and Kidney Diseases (P30 DK34987 to R. Sandler, pilot award to A.D.G.), and the Emory University Department of Medicine (start-up funds to A.D.G.). K.P.A. was supported by the National Cancer Institute (T32 CA071341). The Microscopy Services Laboratory, Department of Pathology and Laboratory Medicine, is supported in part by P30 CA016086 Cancer Center Core Support Grant to the UNC Lineberger Comprehensive Cancer Center.